CHALMERS
UNIVERSITY OF TECHNOLOGY

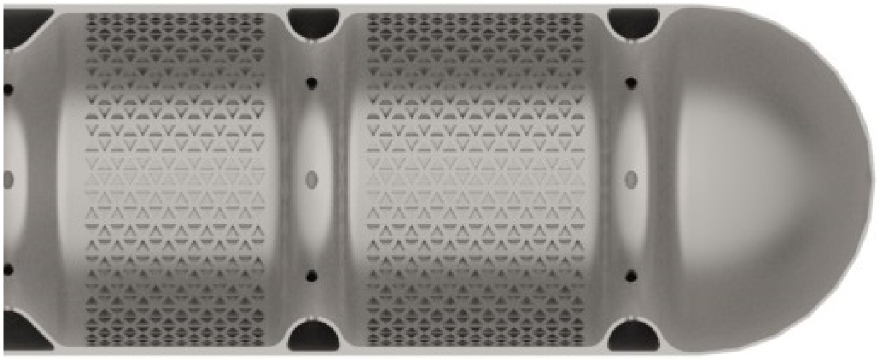

Enhanced performance of magnetic floating devices enabled through metal additive manufacturing

A comprehensive study to enhance buckling performance of thin wall structures through metal additive manufacturing

Master's Thesis work in materials engineering masters program

BHARAT MEHTA

Department of Industrial and Materials Science
CHALMERS UNIVERSITY OF TECHNOLOGY
Gothenburg, Sweden 2019

MASTER'S THESIS 2019

Enhanced performance of magnetic floating devices enabled through metal additive manufacturing

A comprehensive study to enhance buckling performance of thin wall structures through metal additive manufacturing

BHARAT MEHTA

Department of Industrial and Materials Science
Center for Additive Manufacturing (Metal)
CHALMERS UNIVERSITY OF TECHNOLOGY
Gothenburg, Sweden 2019

A comprehensive study to enhance buckling performance of thin wall structures through metal additive manufacturing
BHARAT MEHTA
Master's Thesis work in materials engineering masters program

Supervisor at Chalmers: Marie Fischer, Industrial and Materials Science
Supervisors at ABB: Frédéric Tholence, Erik Johansson
Examiner: Eduard Hryha, Industrial and Materials Science

Master's Thesis 2019
Department of Industrial and Materials Science
Center for Additive Manufacturing (Metal)
Chalmers University of Technology
SE-412 96 Gothenburg
Telephone +46 31 772 1000

Thesis work was performed in the framework of Centre for Additive Manufacturing - Metal (CAM^2) in collaboration with ABB Corporate Research, Västerås, Sweden.

Cover Image: A half-cut section of a modified magnetic floating device, which has been optimized for higher buckling loads and can be printed using additive manufacturing

Gothenburg, Sweden 2019

Enhanced performance of magnetic floating devices enabled through metal additive manufacturing
BHARAT MEHTA
Department of Industrial and Materials Science
Chalmers University of Technology

Abstract

This master's thesis work is focused on establishing the functionalities that can be achieved by utilising additive manufacturing in products currently manufactured using traditional techniques. Additive manufacturing is seen to be a game changer in the current manufacturing scenario. With the fact that complex parts can be made easily and higher design freedom is available, it is possible to push design and material limits further by employing concepts such as lattice structures and topology optimised structures in order to obtain higher strength to weight ratios. Hence, a primary study into the designability of a magnetic floating device was done. It was followed by a secondary study into the mass-manufacturability aspect which is mostly affected by printing parameters.

For this master's thesis work, a family of products which work as floating devices, currently being manufactured at ABB, have been selected to investigate and develop a mass-manufacturable design which can provide much higher specific buckling strength than the current manufacturing methods. It was critical to keep the products similar or better in all performance characteristics (such as corrosion resistance, temperature performance, surface roughness, etc.). The investigation was not limited to using additive manufacturing but rather to suggest optimised techniques to design and manufacture the product family. The material used to study in this thesis was 316L stainless steel, since ABB typically uses the same material for manufacturing the product and it was readily available for additive manufacturing. As a result, several stiffened structures were shown for this product, which were simulated to show significant improvement in performance and manufacturability, improving the specific buckling strength by about three times the current part. From the experiments conducted, a relation between the failure mode of thin shell under uniaxial compression was developed and tailored properties of lattice structures were also studied. Furthermore, an extended study into the effect of laser power, layer thickness, laser speed and scan strategy was also conducted to understand the mass manufacturability of thin cylindrical shells.

Keywords: Additive manufacturing, laser powder bed fusion, thin wall shells, lattice structures, LPBF process parameters, 3D printing, 316L stainless steel

Acknowledgements

This master's thesis work has been a long journey in order to reach here. Firstly, I am immensely grateful to my parents for their ever lasting belief in me, all through my education and sparing no costs to let me do what I wished for. Then, I would thank Eduard Hryha and Santanu Singha for considering me for this thesis. All my supervisors at ABB and Chalmers; namely Marie Fischer, Frédéric Tholence and Erik Johansson for putting up with all my many mistakes throughout the journey and having the patience to not throw me out. Finally, I dedicate most of my work to Jyotika, for being there, always listening to me and bearing with me for all these years.

The thesis work was performed in the framework of the Centre for Additive Manufacturing – Metal (CAM^2), supported by Vinnova.

Bharat Mehta, Gothenburg, June 2019

Contents

1
Introduction

The concept of Additive Manufacturing (AM) is not new. Making products by joining materials has been around for thousands of years. Ways of manufacturing such as stitching or knitting of textiles are good examples. Yarns of textiles are woven together to make certain products such as clothes. The commercialisation of additive manufacturing (or 3D printing) began in the 1980s with the invention of selective laser sintering, stereolithography and fused deposition modelling[1]. This enabled the use of layer by layer manufacturing which was initially used to manufacture prototypes for the industry since the material costs were high and the technology did not have enough resolution and accuracy to compete with conventional manufacturing. Over time, research into improvement in materials, processes and strong competition has brought down the costs to levels where it is closely competing with conventional manufacturing. In the modern world, ASTM[2] defines additive manufacturing as "a process of joining materials to make parts from 3D model data, usually layer upon layer, as opposed to subtractive manufacturing and formative manufacturing methodologies". This enables the designer to print parts which can be used directly out of the printer with less post processing and offer higher design freedom.

Up to now, additive manufacturing has enabled the innovations in design of products in the aerospace, medical and defence industries. It is now extending it's benefits into other industries such as automotive and electrical. Metal additive manufacturing is still developing rapidly with new materials and processes coming up and improving the quality of the final products. For this master's thesis, the product at hand involves a metallic buckling resistant floating structure involving thin shells (sub millimetre thickness) which are welded together. The goal is to improve the device's performance and manufacturability. The design of one of the floats in 316L stainless steel was chosen to be demonstrated as a buckling resistant structure which could be manufactured using additive manufacturing. The CAD models were developed on Solidworks 2017 and the analysis was done on ANSYS V19. The additively manufacturable parts were sliced using Materialise MAGICS 23.0. The manufacturing process was limited to laser based powder bed fusion.

The design work was further supported by experimental work involving small compression tests of thin cylinders, lattice structures and hydrostatic test of cylindrical pieces to establish various offsets from expected material and mechanical properties under linear buckling. To look at mass manufacturability, a secondary study into optimisation of laser process parameters in thin shells with diameter to thickness ratio of as high as 40:1 was also done. The prints of the experiments were done at AMEXCI, Sweden, on an EOS M290 and at ABB Corporate Research, Sweden, on a Realizer SLM 50 printer. At the end, the result and conclusion sections express the various observations derived from the experimental work and how it fits into the design.

1.1 Product background

A metallic floating device is the object of interest for this master's thesis, the details of which are confidential and belongs to ABB, and are hence omitted. This part floats inside a pressurised container and under corrosive and high temperature environments. The part is designed to be so that it has very low specific gravity. Hence, a very low mass/volume ratio is desired for this product to make it float in the fluid medium. This can be done by reducing mass or increasing volume, where increasing volume seems to be the only viable option for the current design, considering there are practical limitations to the thickness of section required to withstand the buckling loads on the part. Then, the part operates under high hydrostatic pressures with a minimum life expectancy of five years having minimal or no maintenance. This particular family of products was chosen because of several reasons:

1. It has an outdated design, which was developed a few decades ago and has not been updated much.
2. There are not any simulations available using the current computational tools.
3. Manufacturing of the product is complex, considering that thin cylindrical shells of metals with span to thickness ratios as high as 100:1 are welded together to make a closed structure which is meeting certain loading characteristics.

This report will explain the fundamental performance indicators of the product and elaborate on how those indicators can be enhanced to result into a better performing product enabled through metal additive manufacturing.

2

Literature Review

This section discusses the literature that was studied in order to understand the part failure conditions and how additive manufacturing approach should be utilised.

2.1 Shell Theory

The product consists of a thin cylindrical shell structure, which can have diameter to thickness ratios of as high as 100:1 and easily qualifies as a thin shell. According to Laszlo[3], thin shells resist the transverse loads mostly by membrane forces, which, at any given point, are in the plane tangential to the reference surface. Hence, the hydrostatic forces acting on the part can be interpreted as the transverse loads and the resultant forces would be membrane forces. Figures 2.1 and 2.2 depicts the same on the membrane of a thin shell.

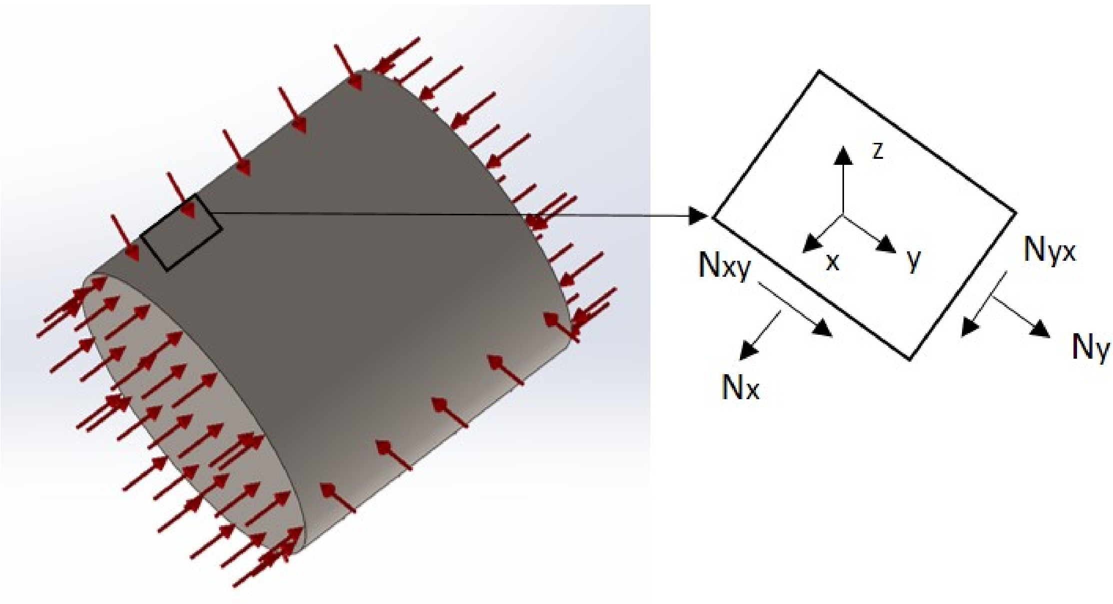

Figure 2.1: Representation of membrane forces on a thin shell surface, redrawn from [3]

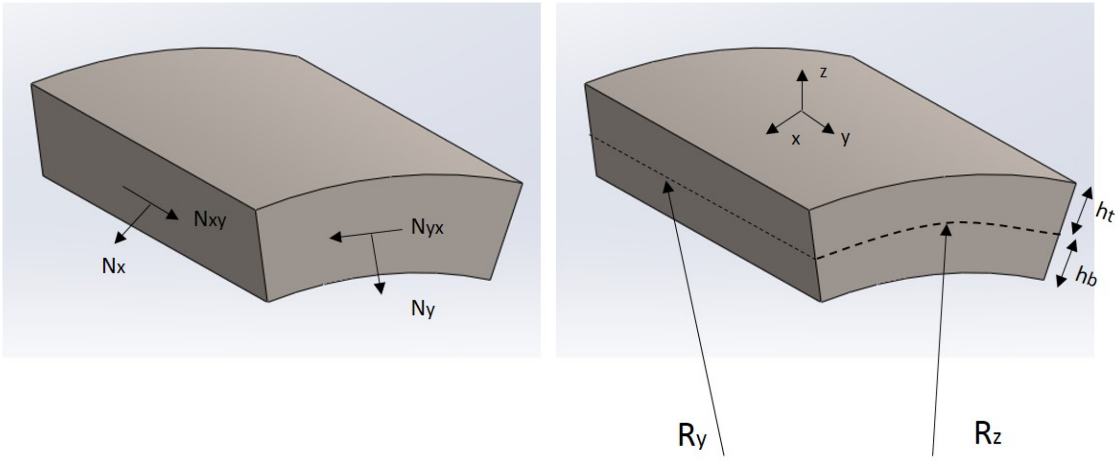

Figure 2.2: Representation of membrane forces and radii of curvature of an element, redrawn from [3]

This means that any bending or shear stresses in the body of the object is assumed to be negligible. This is a simplification of a normal model, which makes it easier to compute the model in simulations. It is based on the assumption that a thin shell whose thickness h is small compared to all other dimensions and with the radii of curvature (as shown in figure 2.2). The formula for the three membrane forces, namely N_x, N_y, N_{xy} can be represented for an infinitesimal element as

$$
\begin{aligned}
N_x &= \int_{-h_b}^{h_t} \sigma_x (1 + \tfrac{z}{R_y}) dz \\
N_y &= \int_{-h_b}^{h_t} \sigma_y (1 + \tfrac{z}{R_x}) dz \\
N_{xy} &= \int_{-h_b}^{h_t} \tau_{xy} (a + \tfrac{z}{R_y}) dz \\
N_{yx} &= \int_{-h_b}^{h_t} \tau_{yx} (a + \tfrac{z}{R_x}) dz
\end{aligned}
$$

where R_x and R_y are the radii of curvature in the x-z and y-z planes, and x,y,z are local coordinates with x and y in the plane tangential and z perpendicular to the reference surface at the point of interest[3]. For thin shells, z/R_y and z/R_x are small as compared to unity. Thus, the expressions above reduces to

$$
\begin{aligned}
N_x &= \int_{-h_b}^{h_t} \sigma_x dz \\
N_y &= \int_{-h_b}^{h_t} \sigma_y dz \\
N_{xy} = N_{yx} &= \int_{-h_b}^{h_t} \tau_{xy} dz
\end{aligned}
$$

2.1.1 Linear buckling considerations

Euler derived the formula for thin columns loaded in compression in 1744 and explained how buckling occurs in them due to out of plane deflection in columns[4]. Figure 2.3 shows a representation of one such uniaxial compression load case. This theory has a limitation that it holds true only in an elastic column under uniaxial compression. From the figure 2.3, it can be seen that axial compression causes the part to deflect laterally. The failure mode as a consequence of such a deflection is called buckling.

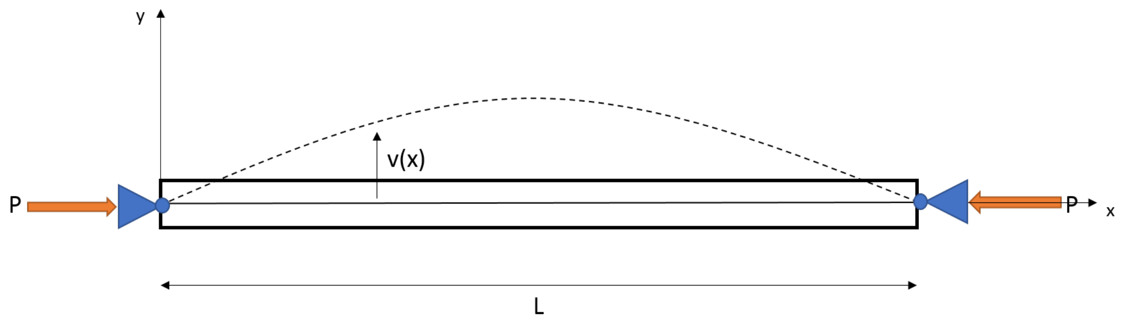

Figure 2.3: A part loaded under uniaxial compression and hinged at both ends; showing a deflection v(x) along lateral direction, redrawn from [5]

Here,
P is the load applied on the part
L is the length of the part
v(x) is the deflection along lateral direction (Y-axis) in the part from origin

As per Euler's buckling theory:

$$P = \frac{\pi^2 .E.I}{(K.L)^2}$$

Where:
P = maximum/critical vertical load on a column
E = modulus of elasticity
I = smallest area moment of inertia
KL = effective length of column (depending on the boundary/loading condition)

Buckling, when occurring linearly, is identifiable and calculable. However, the situation gets complicated when non-linearity comes into picture, which is talked about in section 2.1.2.

2.1.2 Non-linear buckling considerations

The failure mode in the shell need to be considered as non-linear buckling mode because of imperfections formed on the part during manufacturing. These imperfections might show up as distortions caused during welding of thin shells together. The weld itself creates residual stresses and can cause unwanted deformations. Non-linearity is due to the fact that hydrostatic buckling represents plastic failure and the part having surface distortions leads to reduction in critical load that can be taken. According to Amdahl[6], a part under buckling loads does not behave linearly in compressive strain with respect to the compressive stresses. It is generally seen that the small imperfections in the skin of the part can cause detrimental effect on the buckling loads. For example that an imperfection amplitude of only 1/10 of the wall thickness can cause the buckling strengths to be reduced to 60% of the theoretical value(N_{cr}). The figure 2.4 shows the equilibrium paths for perfect and imperfect shells along with influence of axisymmetric imperfections on the buckling load of a cylinder.

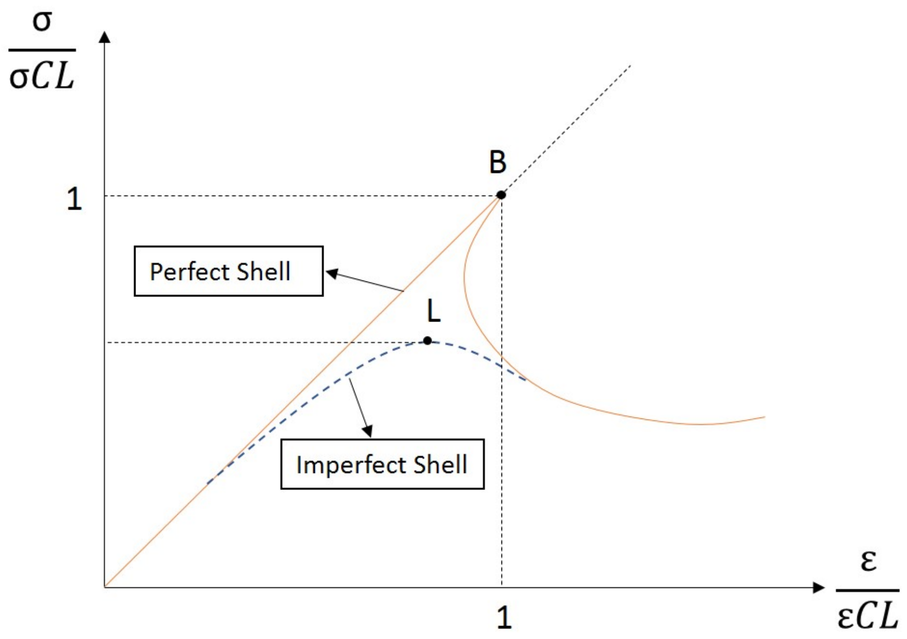

Figure 2.4: Actual/theoretical compressive loads vs actual/theoretical compressive strains for perfect and imperfect shells showing the effect of non-linearity on buckling load bearing capacity, redrawn from [6]

Buckling works in a way that $N_{cr} = \lambda.N$ where N_{cr} is assumed to be the critical buckling load and λ is the load multiplier (as named in ANSYS or Eigen values, as it is called in linear buckling calculations), and N is the unit load applied on the part. λ is a parameter which can be an indicator for different buckling modes by a simulation model, on the basis of the boundary conditions. This value for λ is normally considered for a linear buckling mode. For example, a small closed cylinder is loaded under uniaxial compression, and a unit load of 1 N is applied in the simulation. The calculation was done for three values of failure in linear buckling and λ is calculated as 105, 157 and 183. This would mean that the first mode of buckling, which is also the weakest, will have a critical load of 105 x 1 = 105 N. The second mode would be 157 N and the third would be 183 N. In a real life scenario, the first one is always considered, since it is the weakest one.
There are ways to include imperfections by providing out-of-plane loads, or pre-stress conditions to simulate a more non-linear form of buckling. It is to be noted that these pre-stress conditions should be representative of the actual conditions on the part, to get a "closer to reality" scenario of the buckling failure. Since the first three modes of buckling were considered, it resulted in three values of λ in increasing order. And the first value reflects the failure mode of the part, since it reflects the least load taken to cause buckling. In a few iterations, however, multiple values of λ were considered if they were very close to each other in magnitude.
So, in simple terms, it can mean for the structure that if the unit load is applied as the collapse pressure of the part, it would be required to be at least 1 if it is

assumed to be a perfect shell in order to be safe enough for design loads. But, for an imperfect shell (which is a more realistic case), an extra factor of safety will have to be kept in mind, as for nonlinear buckling, the N_{cr} gets affected drastically. After simulations of the part, which is the case selected for this thesis, simulations reflected a minimum λ of about 1,7 at collapse pressures, which is shown later. However, these values seem to be conservative, since this would correspond to about 10% error in thickness. A 10% error would correspond to about $\pm$0,08 mm in surface inaccuracies. It is assumed that printing will cause about the same error on the surface since 0,08 mm is considered to be the average surface roughness of additively manufactured parts in steel before shot peening[7], whereas the parts are always post-processed after manufacturing, bringing down surface roughnesses to $\pm$0,03 mm even. Hence, $\pm$0,08 mm, being a conservative value was selected as the reference value.

2.1.3 Modification to the part and need for ribs/stiffeners

After establishing the basic theory behind the work and the model of the part, the next thought would be how to get a stronger part, without increasing the weight drastically. For understanding the same, stiffeners in cylindrical shells were studied. A comparison between the commonly used longitudinal and circumferential ribs as stiffeners and the resultant buckling modes was done. These buckling modes were kept in mind for comparison with simulations[6]. In the current part, ABB adds ring stiffeners since they are helpful in reducing the amount of deflection in the unsupported area. The ring stiffeners restrict the deflection in the whole tube and makes it resistant to buckling [6].
The simulation for the first mode of Euler buckling failure for an empty tube was done. Then, a comparison with parts having 6 longitudinal ribs, 5 weld rings and both of those followed. The end results were interesting to note and corroborate with the theory, as shown in table 2.1.

Table 2.1: Table reflecting the mode of failure and the corresponding factor of safety for the tubes with different stiffeners

First mode of failure	Buckling factor of safety
Only tube	1,11
Tube with 6 longitudinal ribs	1,18
Tube with 5 weld rings	5,71
Tube with both longitudinal ribs and weld rings	11,94

The figure 2.5 represent the buckling failure mode in the different load cases.

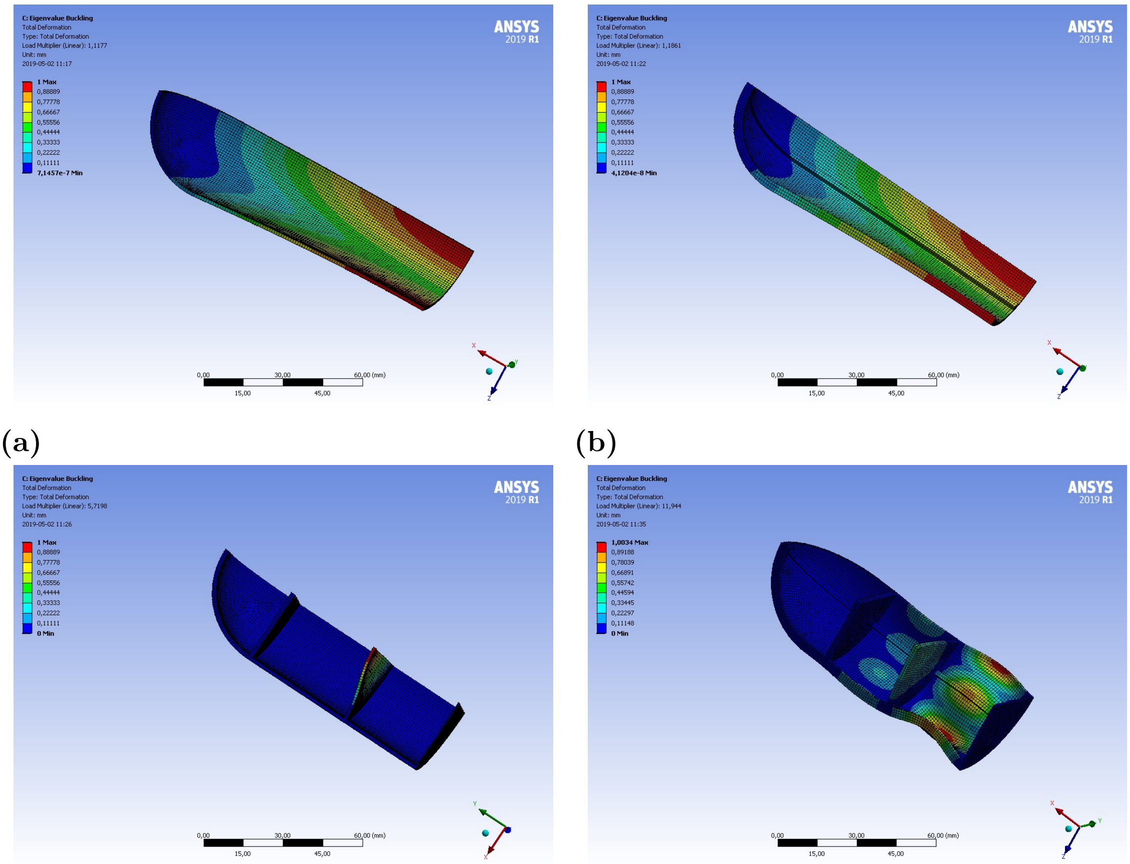

(a) (b) (c) (d)

Figure 2.5: λ or buckling factor of safety comparison between sections with different stiffeners under hydrostatic loads: a) λ for an empty tube; b) λ for a tube with longitudinal ribs; c) λ for a tube with only 5 weld rings; d) λ for a tube with longitudinal ribs and weld rings

Overall, it can be seen that the strength to density ratios get affected. Figure 2.6 is an Ashby chart reflecting on how the part performance is improved with rings and ribs (a part higher on the slope of strength/weight is considered to be a stronger part). If there is a certain minimum performance requirement from the part (as depicted by the blue shaded area) such as high buckling strength or low weight, adding certain stiffeners can improve the part's performance.

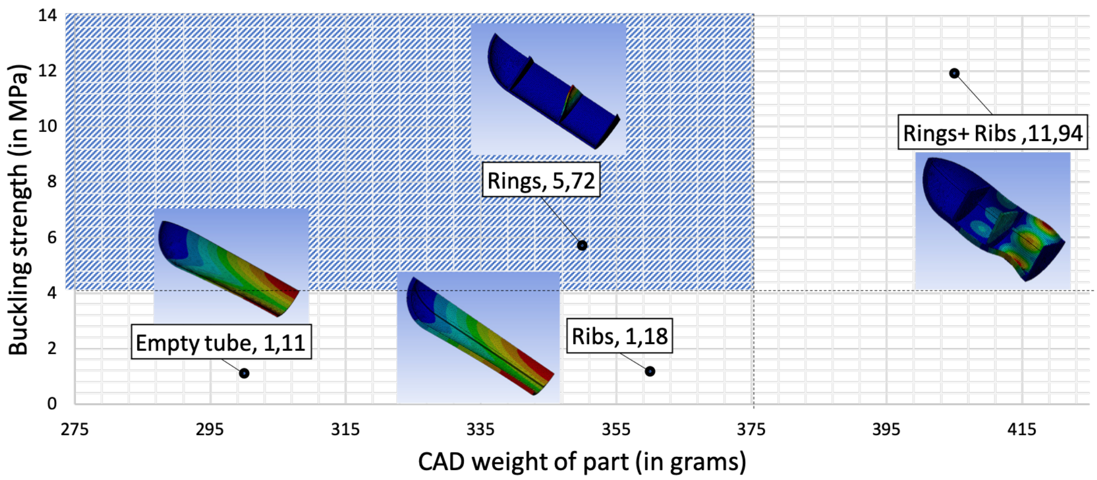

Figure 2.6: Ashby chart[8] for reflecting strength/weight ratio of the tubes with different stiffeners

It was evident from understanding the theory that the impact of the ring stiffeners is most effective, but when used in conjunction with longitudinal stiffeners produce the best result whereas using longitudinal ribs alone does not prove to be very useful. The use of both the stiffening mechanisms together gives best performance, though it can be problematic due to increase in the weight. Hence, it would be better to utilise the best of both concepts and stay within the required limits of weight.

2.2 Introduction to additive manufacturing

ASTM[2] defines additive manufacturing as a process of joining materials to make parts from 3D model data, usually layer upon layer, as opposed to subtractive manufacturing and formative manufacturing methodologies. This advantage helps the CAD designer to get rid of conventional manufacturing problems such as drafts, undercut, etc. There are other benefits such as control of microstructure in metal AM, possibility to print lattice structures or internal channels to enhance designs and save a lot of material wastage by building near-net shape parts. However, there are other additional limitations while employing AM techniques, such as residual stresses, requirement of supports while building, not enough materials available for printing, etc. All AM technologies can be categorised into seven technologies:

1. Vat photopolymerisation
2. Powder bed fusion
3. Material extrusion
4. Material jetting
5. Binder jetting
6. Directed energy deposition
7. Sheet lamination

For metals, the technologies of interest are powder bed fusion, directed energy deposition and binder jetting. And for producing parts with very small wall thicknesses, high surface quality and high dimensional requirements, powder bed fusion is the only technology of choice. Metal powder bed fusion can be characterised by “layer by layer” melting of powder by using focused lasers or electron beams in specific chambers. These chambers can be filled with inert gases such as N_2 or Ar for laser beams or kept in vacuum in case of electron beams[9][10].

After some discussions about both these technologies, it was collectively decided to keep this thesis concentrated towards laser based powder bed fusion(LPBF) and not electron beam based powder bed fusion. LPBF was chosen owing to the availability of the 316L stainless steel powder and the machines at both ABB and Chalmers. Hence, this thesis focuses on LPBF and thus the processing and benefits/drawbacks were derived from LPBF. Furthermore, several benefits and limitations to using the AM technology of choice, some of which are specific to the floating device were discussed in following sub sections.

2.2.1 Benefits of AM

Additive manufacturing is seen as a good candidate since it has the ability to resolve many manufacturing issues and at the same time, has the possibility to overcome the design limitations of the part. For this particular product, metal LPBF helps in the following way :

1. It is seen that the manufacturing complexity involving complicated welding/joining of several parts could be reduced down to fewer parts, which will implicate lesser defects and easier assembly.
2. Since the geometry produced using AM would be accurate, the need for post processing afterwards will decrease.
3. The design requires certain amount of rigidity in the shell to meet high pressure requirements (as high as several hundred bars). AM can provide innovative ways to improve this structural rigidity through the use of lattice structures or reinforced structures inside the part, which is not possible through conventional manufacturing. This can have the benefit of reducing weight on the final part, which is beneficial.
4. As per Matilainen[11] the weldability and quality of overall weld with the microstructure formation are considered at par with welded sheet metal parts in 316L stainless steel.
5. The customisation based on customer requirements can be made possible by AM, drastically reducing manufacturing lead times as parts with different specifications can be built together. It can be a clever way to manufacture parts on demand.

2.2.2 Limitations of AM

Like any other technology which is considerably new, AM has it’s limitations as well. Thus, the following need to be kept in mind while deciding to go for metal AM:

1. The metal AM process involves higher surface roughnesses, up to ±80 µm for as manufactured parts, which should be investigated.

2. Fewer materials are available for metal AM. The normal manufacturing processes have hundreds of alloys available for use, whereas AM has only about 20-30 materials available. However, the trend of developing new materials for use in AM is expanding rapidly[12].
3. The manufacturing times for AM can be high, since printing is done layer by layer and it increases rapidly when the part height is increased. Normal LPBF processes have building speeds of about 5-20 cm^3/h[13], which is considered slow compared to conventional manufacturing methods.
4. Since the printing process depends on so many different factors such as laser power, laser speed, hatching strategy, angle to build plate etc., it is difficult to produce consistently good parts with similar properties. However, machines are developing fast and industrial grade machines are being made available by companies such as EOS, SLM solutions.

2.3 Design for additive manufacturing

Design for additive manufacturing (DfAM) is an upcoming field within additive manufacturing which involves developing ground rules/ design limitations of AM for various processes and reap the real benefits of this technology. Many times, it is mistakenly assumed that anything can be made using additive manufacturing, which is completely wrong. Like any other manufacturing process, AM has it's constraints. These constraints are new and need to be formulated in a different way than conventional design methodologies. It is also noteworthy that many older design flaws can be overcome and new designs inspired from nature (also called "bionic designs") can be incorporated into products making their value increase due to improvement in aesthetics and performance.
This subsection will discuss some characteristics to keep in mind as design guidelines while designing for AM components. Several guides are available for beginners to understand the details of DfAM. It is explained with example, in [14] Renishaw's beginner's guide to AM. There are four critical factors which affect the AM design and can be taken as the basic thumb rules while doing any kind of designs:

1. Residual stress:
   Residual stress is an unavoidable circumstance, which can "make or break" an AM build. It is formed due to rapid heating and cooling after the laser pass on unmelted powder on each layer. Continuous melting on 20 µm and 40 µm layers of build after every 30-100 seconds on each layer, causes a lot of concentrated energy transfer into the melt. In extreme cases, this stress can exceed the strength of the material, thus causing distortion or even failures in part during printing. These stresses are avoided by changing the path that the laser follows (also called scanning strategy) in order to avoid overheating in local areas of the build platform. Another technique is to heat the build plate in order to keep a lower temperature gradient between layers while printing and thus reducing the residual stresses. For example: a temperature of about 80 ℃ is kept for parts while printing 316L stainless steel in a typical EOS M290 machine. The figure 2.7 shows a failure seen during one of the prints at ABB, due to residual stress and not having strong supports.

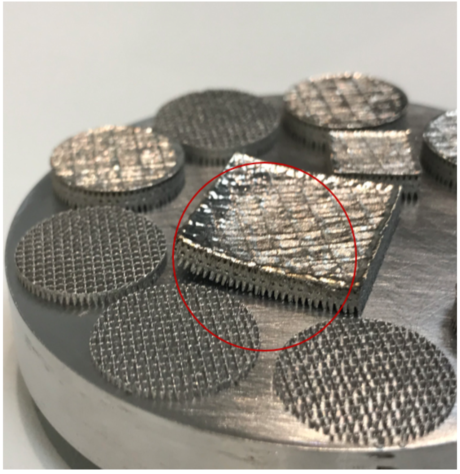

Figure 2.7: Failure in printing due to residual stresses

2. Orientation:
   Any additive layer based process is defined along Z-axis (also known as build direction). There is a need to modify the build orientation in an additively manufactured part, since the cross section of the part may not be optimised for the print. Some of the reasons why the cross section of the layer can be of importance to optimise are as follows:
   (a) Overhangs:
   The layer based AM printing processes depends on the preceding layer to the one being printed, to provide both, physical support and heat conduction away from the part. As per [14], heat would flow from the melt pool down to the build plate during the printing process. The melt pool solidifies quickly once the laser source has passed as heat is conducted away from the build. When there are overhangs, both these conditions are not fulfilled and leads to rougher surfaces and residual stresses. This limits the possibility of having big overhangs, and necessitates the use for supports structures to be able to print the part as required. A clever solution is to have fillets or chamfers to reduce stress and make it possible to print overhangs.
   (b) Orientation from build plate :
   A general rule of thumb says that the printing of the part cannot be done with surfaces oriented less than 45° from the build plate. If these angles are decreased, the down surface (down skin) can have a rougher surface or develop stresses due the the slower cooling of the melt pool below (Since the melt pool is not supported by solid material, rather by lose powder or less dense supports). Here, a clever way to designing could be to redesign the initial component to make it self-supporting.
   (c) Orientation of features :
   The orientation to the moving recoater blade is also an important factor to consider while printing. As per [14], when a new layer of powder is applied, the recoater compacts the powder in a consistent layer so that a densely packed layer is formed. This necessitates the build to be free from

residual stresses and stay flat; at the same time it forces powder down and pushes the front edge of the component upwards as the recoater crosses over the part. The way to overcome that is to use a flexible recoater having rubber or carbon brush instead of steel. Although, having a flexible recoater may lead to rougher surfaces.

3. Support structures:
   The supports that are added to the design for taking away heat or being able to print overhangs has its own limitations. They come with the cost of bad surfaces or difficulty in removal from the part after printing. Supports might also be necessary for part features such as big holes perpendicular to build plate, where distortion in the hole can occur unless support is provided. Sometimes, a clever way to incorporate holes is to print smaller concentric holes and machine afterwards. The figure 2.8 shows how support structures can be used on an existing overhang.

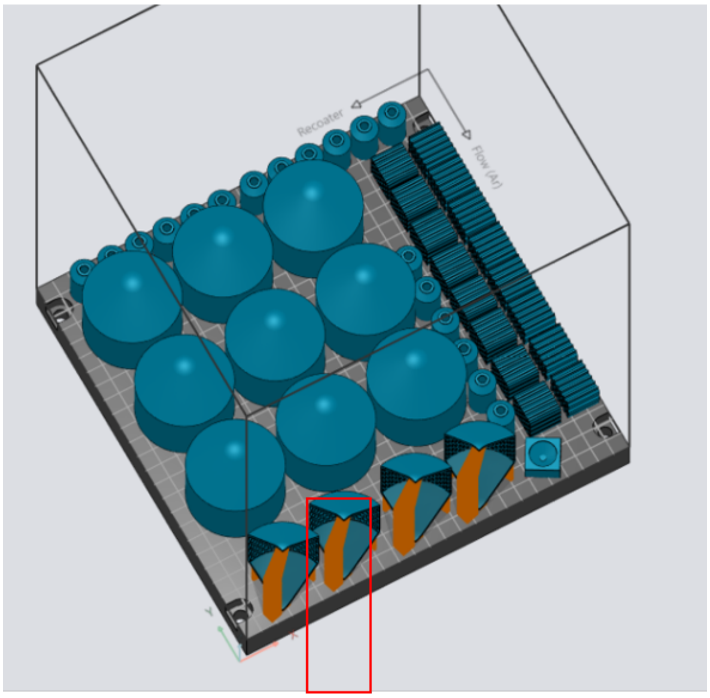

Figure 2.8: Importance of support structures to deal with overhangs

4. Optimisation in part design:
   There are several optimisation principles that are directly applicable to AM, such as topology optimisation[15] or printing lattice structures[16] to bring higher specific strength and elasticity by creating a kind of hybrid material with air and the base material. The idea to keep in mind is that AM involves rough surfaces and these optimisations are limited, making it quite difficult to consistently manufacture high quality products with comparable properties. The build times get directly affected by increasing vertical (Z-direction) height during printing and make it complex to provide higher rates of production. Standards are gradually being implemented to manage properties and machine manufacturers are working closely with process parameters for product and

productivity control.
Hence, DfAM is a critical factor, which is to be considered while designing parts. Since the part is planned to be mass manufactured in metal AM, these factors are good from a theoretical point of view. If proper design guidelines are not followed, results can be disastrous, leading to printer crashing after a 50 hour print, like the one shown in figure 2.9.

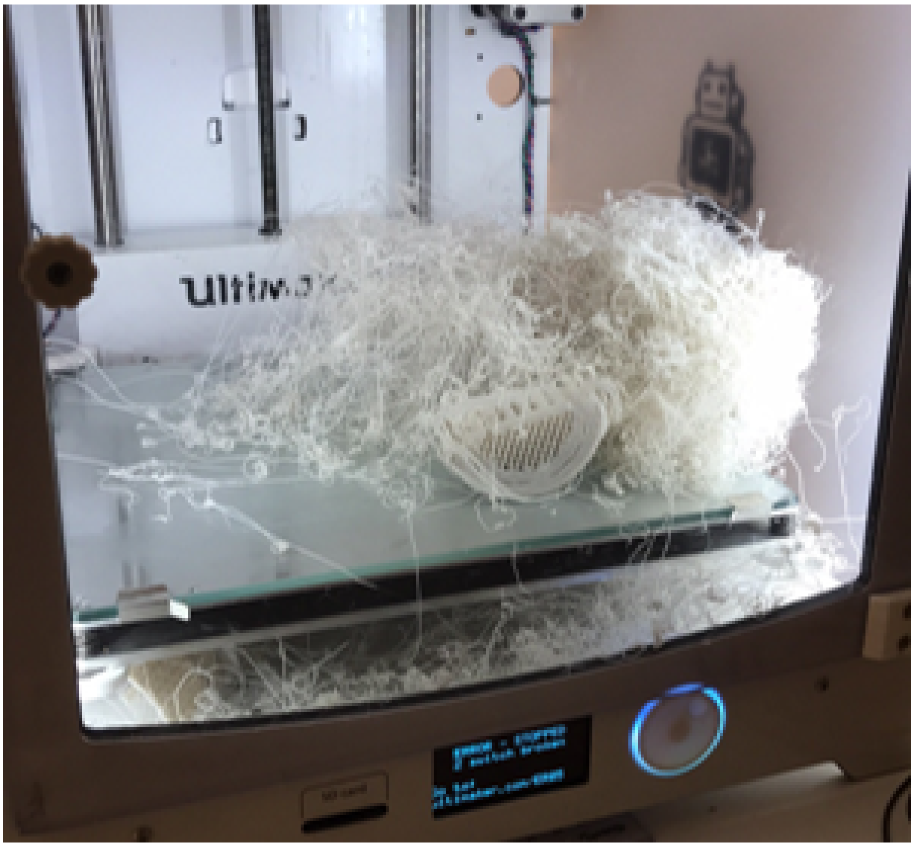

Figure 2.9: Print failure for a plastic print job that was planned for 50 hours with no usable parts left

2.3.1 Lattice structures and topology optimisations

2.3.1.1 Lattice structures

As per [17] crystal structure is the periodic manner in which atoms, ions, or molecules are spatially arranged. The smallest group for this repeating pattern is called a unit cell. For structural applications, these unit cells can form a long range order to meet specific requirements such as having certain specific strength, elasticity or anisotropic properties. For the given product, it was thought of providing extra stiffness along the build direction (Z-direction) and against hydrostatic loads (Y-direction) by using cleverly designed lattice structures, which are projected on the surface of the part. These will help retain the weight ratios and work as stiffeners to the part. For lattice structures, if the discussion delves into material property charts, it becomes visible as to how the lattice structures are desirable from a designer's point of view. Figure

2.10 shows the Ashby chart for tensile strength vs density, which reflects the wide variety of materials available to choose from. Here, graphical selection of a better material can be done based on a certain performance parameter (in this case, being a higher strength/density ratio).

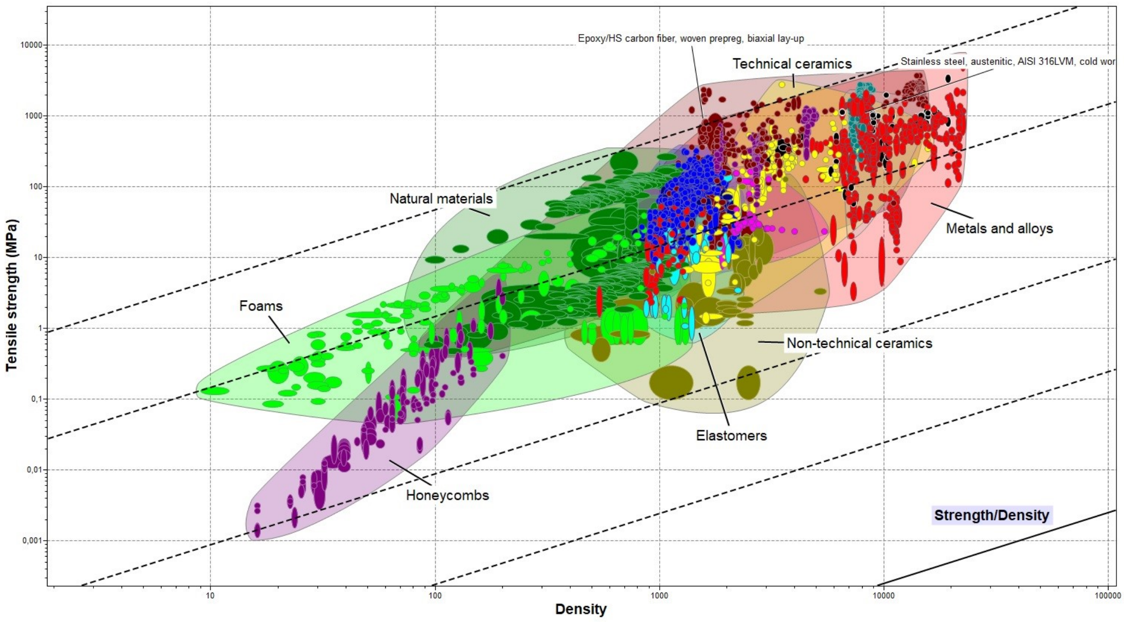

Figure 2.10: Ashby chart for tensile strength vs density for different materials[8]

Now, 316L stainless steel and a epoxy/HS carbon fibre are compared (assuming that both 316L stainless steel produced using AM has similar properties as wrought part) for the design of a strong beam, where higher $\frac{\sigma}{\rho}$(strength/density) values are desired. It can be seen that they have similar strength (σ) values, whereas epoxy/HS is much better because it has much lower density.
If lattice structures are used for steel here, it would have the possibility to reduce the part density to as low as 10% of the original part. If a smart lattice can be produced, retaining the directional strength of the original part or meeting design loads, while at the same time reducing the density (to about 30%), then better strength to weight ratios than carbon fibre composites may be achieved.

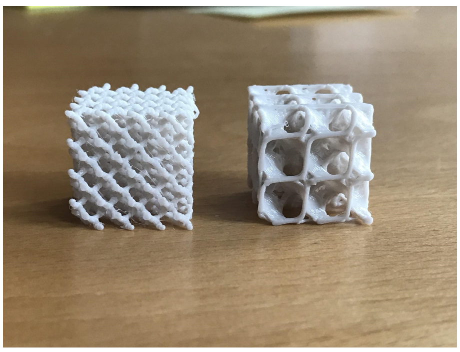

Figure 2.11: Example of diamond structure and schwarz-D structure to represent how a lattice structures looks like

2.3.1.2 Topology optimisation

Topology optimisation in principle refers to the ability to define the part design based on the load path and resulting stress distribution, leading to removing excess material based on volumetric or weight redistribution. As an example, a component optimised for a formula student vehicle was studied.[15] They talk about how a part being milled in aluminium 7075 is taken and the loads are identified, based on which a topology optimised design is developed to transform it into a part printable for additive manufacturing in Ti6Al4V. Doing that, a weight saving of 36% was achieved, which is remarkable. The overall weight savings is shown in table 2.2.

Table 2.2: Comparison of machined component to additively manufactured one[15]

Assessment criteria	**Machined aluminium**	**EBM titanium (Ti6Al4V)**	**% Change**
Mass, grams	832	536	-36%
Factor of safety	0,95*	1,70**	+79%
Maximum displacement, mm	0,25	0,32	+28%
Raw material use, kg	7,0	1,0	-86%
Cost of manufacture, GBP	342	2980	+773%

*w.r.t yield strength. **w.r.t fatigue limit at 10^6 cycles

By combining these techniques for laser based metal AM technologies, a highly optimised part may be achieved. It will perform much better and will weigh much less. In the case of the floating device, the part is loaded with hydrostatic pressure from the outside of the shell. It basically means that there is constant force across the whole part surface which is trying to crush the part inwards. The representation in figure 2.12 reflects a similar load case.

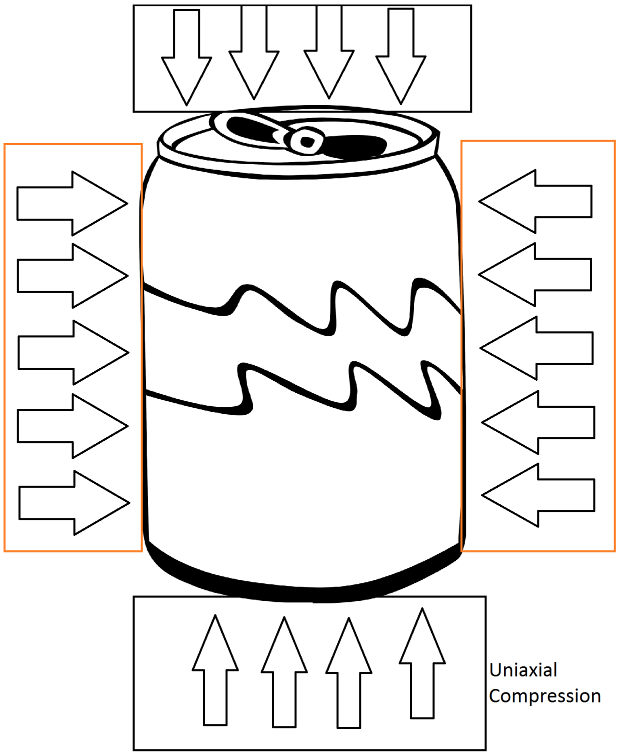

Figure 2.12: Representation of hydrostatic load on a soda can

This was a challenge to optimise, considering a part is made of sub-millimeter thin sheets of steel. However, through AM, innovative ways were employed to reinvent the structure. The skin was reduced to about half its thickness and then some "stiffeners" in the form of lattice structures were added to support the loads generated by these hydrostatic forces.[6] After some literature study of stiffeners used for buckling resistant structures and from the ANSYS simulations that were studied, concepts that were used were discussed.

1. Honeycomb design:
   Honeycomb structures are based on honeycomb design, where a hexagon is used as a 2-dimensional lattice and can be extruded into 3 dimensions, to create a very stiff and low density structure. These structures are resilient to bending and compression forces, thus making them good for buckling resistant structures. These kind of properties, combined with a high positive poisson's ratio along the direction of the honeycomb structures were an important reason for considering honeycombs as stiffeners. These honeycomb structures are employed in aerospace and automotive applications to enhance part properties and get stiffer and stronger parts in compression, which fits our criterion. There was only one challenge: the honeycomb that was designed for this part had to be self supporting in the direction of AM print (Z-direction) since the part was planned to be printed vertically. Hence, the honeycomb structures were tweaked to have higher vertical angles of about 45 degrees from the horizontal and thus look elongated as seen from the picture below.

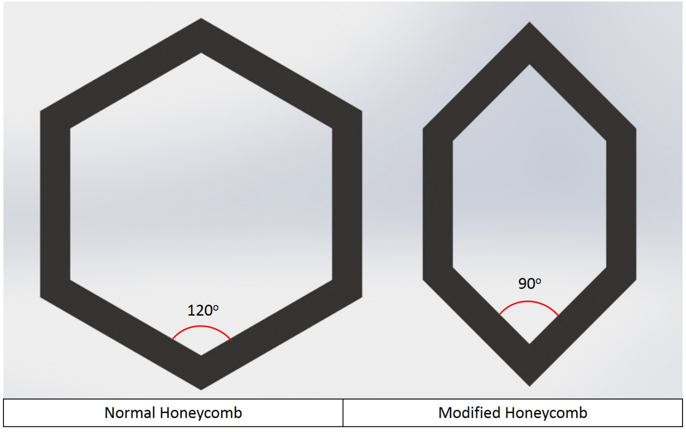

Figure 2.13: Comparison between normal honeycomb and modified honeycomb

2. Grid based structures:
   There are several types of grid based structures available, such as isogrids, anisogrids [18] and orthogrids, to name a few. Some of them are represented in figure 2.14.

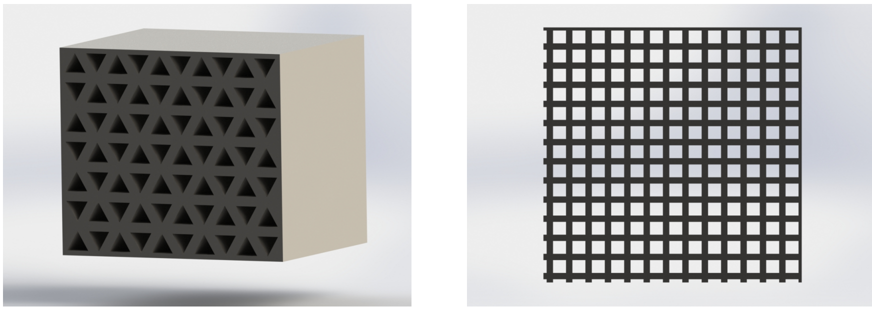

(a) **(b)**

Figure 2.14: Examples of grid based structural lattices: a) isogrid structures and b) orthogrid structures

The benefits of using these structures are to have an improvement in buckling load and these kind of structures are quite useful for buckling resistant structures for space crafts. After some simulations and using DfAM techniques, the following was observed:

(a) The anisogrids and orthogrids had more corners than an isogrid per unit area, hence creating higher number of sites for stress concentrations.
(b) The anisogrids and orthogrids were found to be harder to print due to the unfavorable angular orientation of parts in anisogrids and overhangs in orthogrids.
(c) The buckling response of isogrids, as per ANSYS simulations, were found to be the best out of all the three, hence another motivation to choose them.

Some examples of structures where these grid based structures can be found are in real life rocket ships, which companies like Boeing or SpaceX work with [19][20].

2.3.2 Effect of poisson's ratio in selection of stiffeners

The enhancement of performance due to positive poisson's ratio was investigated. It was assumed that the hydrostatic loading can be divided into two parts, as shown in figure 2.12. From the front view, the part has a component of uniaxial compression along Z direction and bending along X-Y plane (radial plane). It was then simulated to prove that honeycombs can be created with high positive poisson's ratio in the direction perpendicular to the uniaxial load application. In the case of this stiffened structure, this would mean that during compression, these structures will "open up" towards the outside when the uniaxial load is applied. This means that, when the part is loaded due to unaxial compression, it tends to expand outwards, which in turn helps against the bending loads on the wall, which is desirable. An ANSYS representation of a honeycomb lattice, along a thin wall section when loaded under uniaxial compression, is shown in figure 2.15.

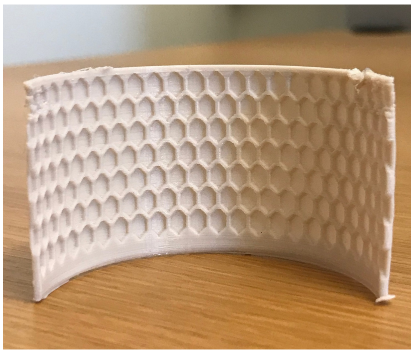

(a)

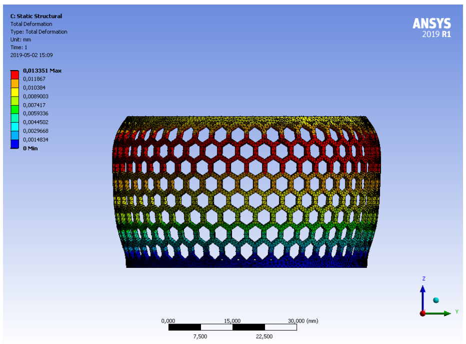

(b)

Figure 2.15: Effect of poisson's ratio in selection of stiffeners for thin shells: a) representation of modified honeycomb as expected to be printed on the thin shell ; b) honeycomb loaded with uniaxial compression, as shown

3
Design, simulation setup and material definition

3.1 Design and simulation setup for baseline part

Several design tools have been employed to CAD and simulate the part in question accurately. Although the part is actually represented by a thin shell, a solid mesh is preferred for defining the part. The reason for that is when lattice structures and different design concepts are incorporated, which are possible using AM, it became increasingly hard to keep following the shell mesh. Thus, the baseline model and all the future models were based on solid mesh for the sake of simplicity. The mesh was further defined as a solid quadratic mesh with hexahedral elements of 1 mm size in order to keep it realistic and not increase the computational time exponentially. The parts were loaded with a pressure of about 7,5 MPa (75 bars) and then a normalised model was developed considering the original part being used as a benchmark.
The part design has not been shared as a part of the report. However, it can be explained as a thin shell cylindrical section which is closed by welding and is supported by some ring stiffeners to make it bear the hydrostatic loads. As a modification to the original part, a slight modification was done based on ANSYS simulation results, producing a simulation based design to thicken the rings. The same was done to avoid the failure at rings and change the load path, in order to get a skin type buckling failure.

3.2 Simulation modified design

After simulating the part, the results of which are discussed later, a simulation modified design was made, with the rings becoming thicker and the holes in the rings becoming bigger, in order to have similar weight. The results of buckling were greatly improved, and are discussed later. To visually represent the modification done, figure 3.1 shows a comparative image to visualise the difference.

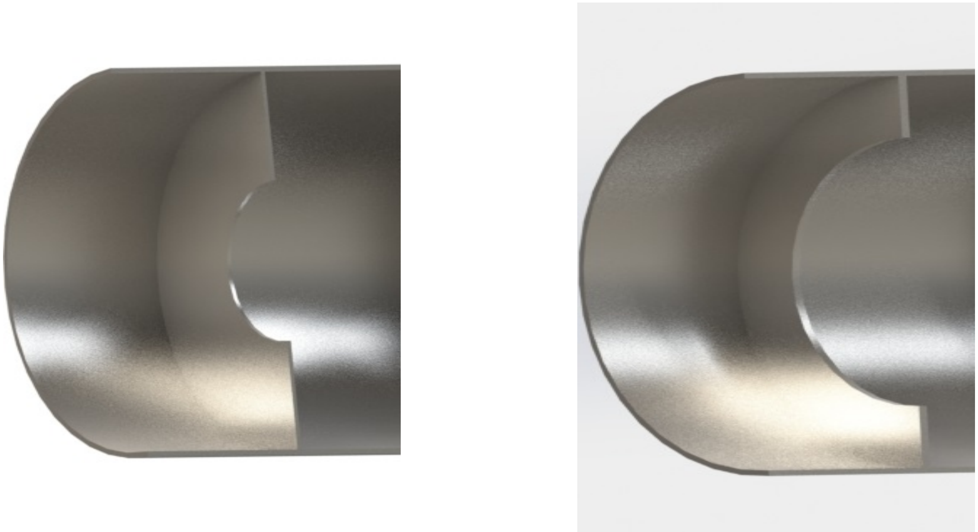

(a) (b)

Figure 3.1: Difference between original ring stiffeners as used by ABB vs a modified ring stiffener : a) the original ring design with 0,5 mm thickness rings ; b) modified ring design with 1 mm thick rings with bigger inner diameter

3.3 AM modified design

The DfAM process of trying to find the best structure was an iterative process of figuring out if the theoretical concepts learnt in literature could be applied to the design, while still keeping the parts printable. So, the first few concepts targeted subjects such as printability and tried to consolidate parts. The part about improving performance was not kept in mind to optimise and the baseline model was kept as reference for weight and performance references. The first few designs are shown in figure 3.2.

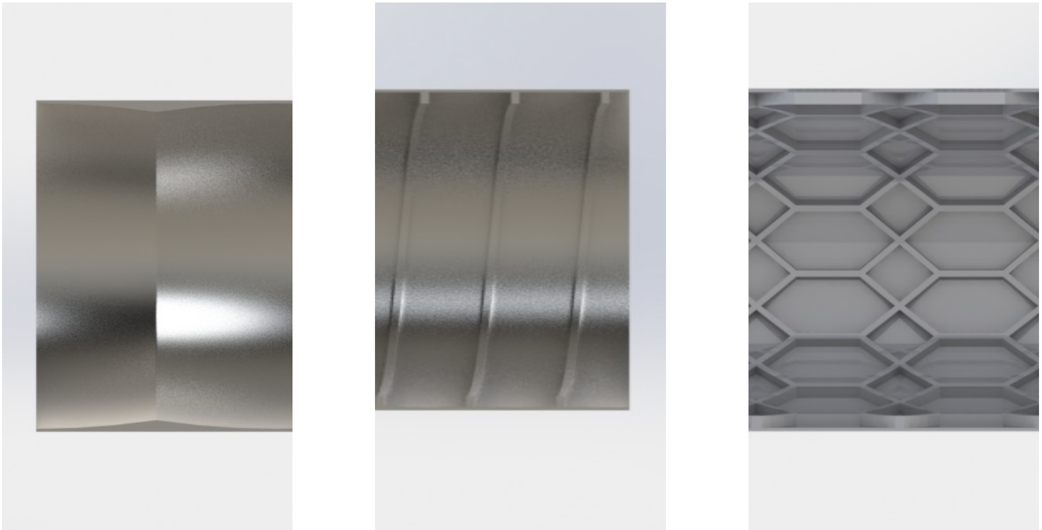

(a) **(b)** **(c)**

Figure 3.2: Different design concepts which are suitable for metal AM: a) with some small protrusions as ring stiffeners; b) with helical supports as stiffeners; c) with honeycombs as stiffeners

After these designs were tried to stiffen the part at a global level, it was realised that local breaks such as the ones provided by the stiffening rings in the original part is a necessity. Hence, the concept of hollow ring stiffeners came into picture. It was also seen that the rest of the part, having a lattice based structure proved to be stronger and stiffer than an empty tube with similar weight. Thus, hybrid designs consisting of both lattice structures and hollow rings were introduced. These designs were printable and provided very high buckling response. A structure with only hollow ring stiffeners is shown in figure 3.3.

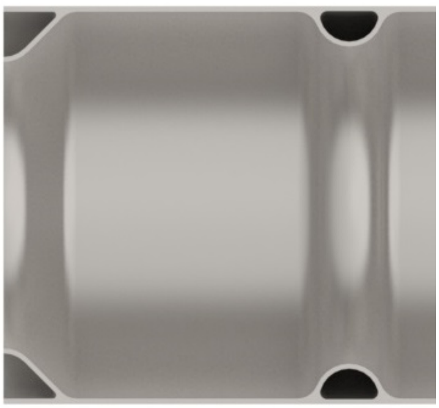

Figure 3.3: Float section with only hollow ring stiffeners

The final float design was then formalised by tweaking the hollow rings' thickness and sizes to get the best ANSYS result and printability as well. Two of such hybrid designs are shown in figure 3.4 and 3.5.

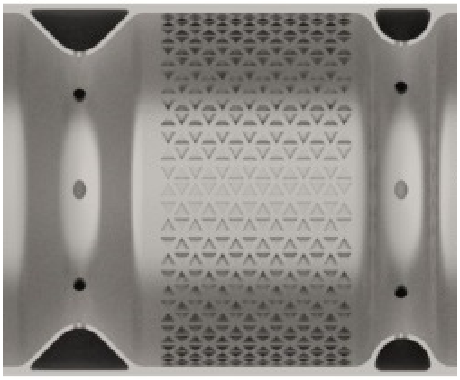

Figure 3.4: Final design of float section with isogrid patterns as stiffeners

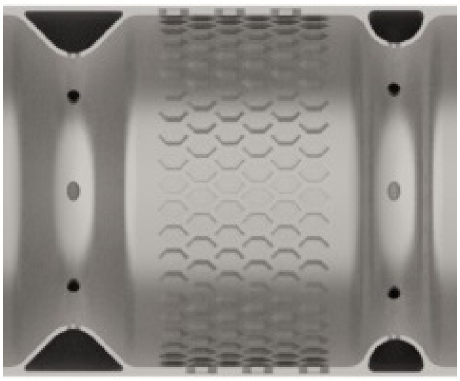

Figure 3.5: Final design of float section with honeycomb patterns as stiffeners

There are elliptical holes provided in the design to remove powder post printing and to keep the stress concentrations minimum on the part. Fillets have also been introduced in the part to reduce the stress while minimising the effect on weight increase.

3.4 Material definition

The original part is assumed to have the properties as provided in ANSYS for 316L stainless steel sheet and the AM part has properties as recommended by EOS[7].

4
Experimental setup

The experimental setup provide the groundwork for establishing the actual performance with respect to the theoretical performance of the AM printed parts, the results of which could be useful. As discussed in theory, linear buckling of the part was not the correct representation to what would actually happen when the part fails. This is because hydrostatic buckling represents a plastic failure and the collapse pressure is used to define the maximum loads for the part. Hence, a sturdier design, which incorporated non-linearity, was planned to be tested and prove the design's performance in real life. Several factors were found to affect the performance while switching to AM, and experimental setups were defined accordingly. The parts for experiment 1, 2 and 3 were printed at AMEXCI on an EOS M290 printer and parts for experiment 4 were printed at ABB on a realizer SLM 50 printer.

4.1 Experiment 1: Uniaxial compression of thin shells

The first experiment was planned to identify the non-linearity induced on a thin shell during uniaxial compression. The variables were the thickness and surface roughness of AM parts and were to be compared to ANSYS results. The parts designed were small, about 30 mm tall, with 16 mm outer diameter and thickness in cylindrical sections between 0,4 and 0,8 mm. Figure 4.1 shows how one of the printed parts looks like on the left side. The right side shows the mating part designed, in order to keep the sample flat on a compression testing equipment.

(a)

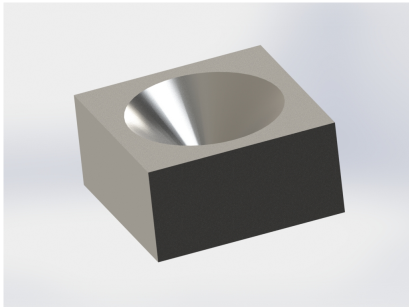

(b)

Figure 4.1: Setup of experiment 1 showing a cylindrical section to be tested and the corresponding female mould to make two flat surfaces for testing: a) cylindrical section to be tested in uniaxial compression; b) mating female part to cylindrical section

Applying DfAM principles, the top of this cylinder had a conical section to make it printable and have a hole to remove the unused powder. Now, for testing under unaxial compression, two flat surfaces are required. In order to achieve that, a matching female mould (as shown in figure 4.1) was planned to align the parts into a straight line and have a decent uniaxial compression test possible. The idea was to observe the buckling mode in the thin section, get the critical load value before failure and compare the same with ANSYS results. The minimum diameter/thickness ratios used were 40:1, which were assumed to be good enough to give a projection on how much effect of surface roughness can be expected on thin shells. However, it is recommended to test these thin shells till a ratio of 100:1 to replicate the non-linearity effect on actual parts. The actual parts were loaded in the universal testing machine (UTM) in a 100 kN load cell and were tested at 1 mm/min. These parts were tested for the first two modes of global buckling, as observed on the part. The experimental setup is shown in figure 4.2.

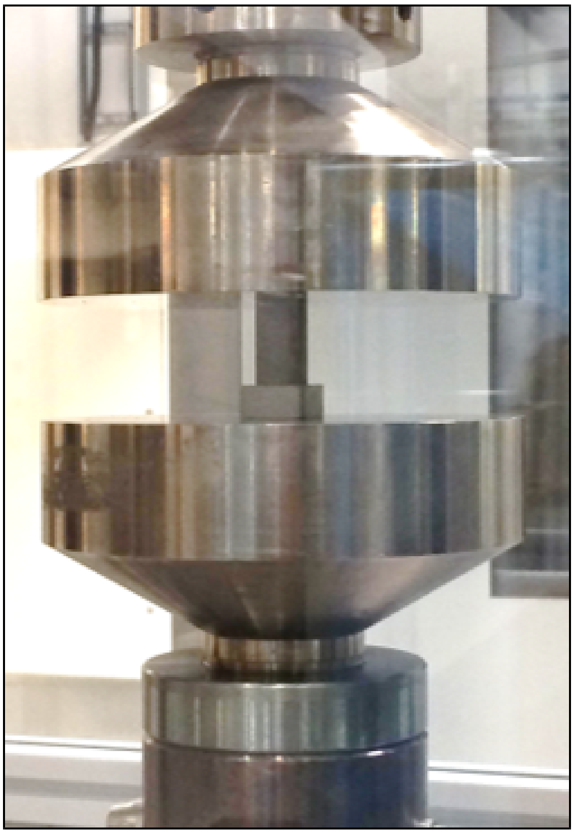

Figure 4.2: Experiment 1 after loading in the universal testing machine with a 100 kN load cell

4.2 Experiment 2: Directional properties of stiffeners

The second experiment was planned to study the directional mechanical properties of the stiffeners, namely honeycomb, isogrids and orthogrids. Since these stiffeners will not only increase the part strength due to radial forces on the outside of the part, it was expected that these stiffeners help with forces along axial direction as well. Based on the same, about 20 mm x 20 mm x 20 mm cubes were designed and were tested. The cubes are shown in figure 4.3.

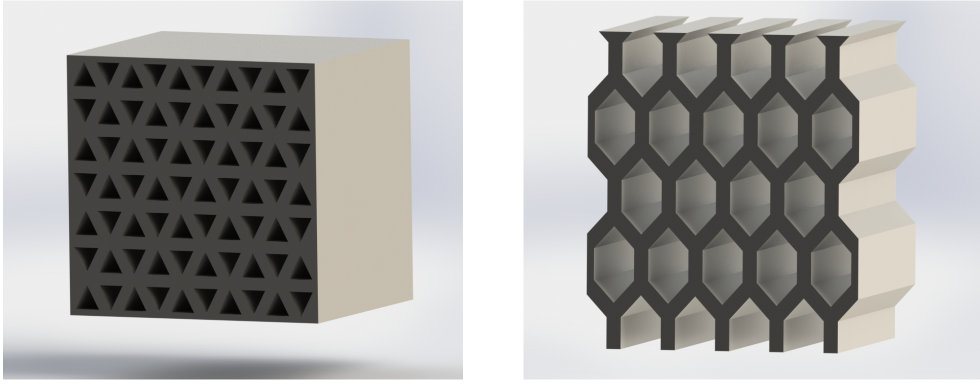

(a) **(b)**

Figure 4.3: Lattice cube representations for experiment 2 showing the CAD geometry for the isogrid and honeycomb lattices to be tested in unaxial compression: a) isogrid lattice cube; b) honeycomb lattice cube

The idea with these lattice cubes is to test them along build plate (X-Y) directions and Z direction separately. The same would provide the load-displacement curves for these stiffeners in both directions and would also reflect the kind of plastic failure that happens in them, since they would be having very thin struts (about 1 mm). These properties obtained using experimentation can then be applied as new material properties to any part to simulate its performance. The experimental setup on the UTM loaded in the same manner as experiment 1, is shown in figure 4.4.

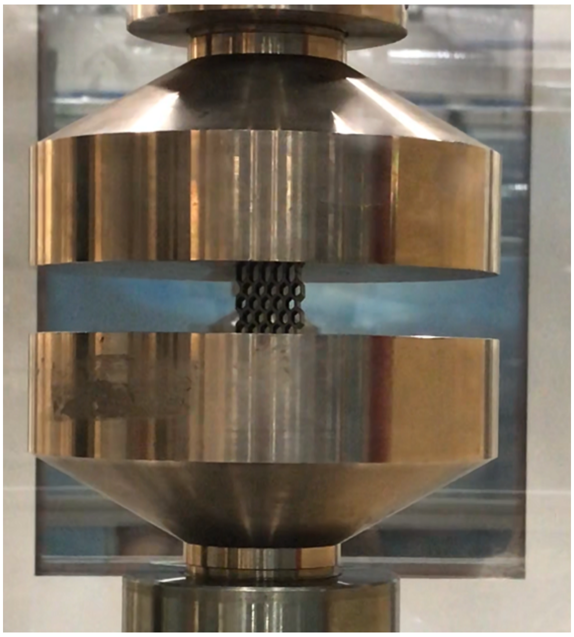

Figure 4.4: Experiment 2 after loading in the universal testing machine with a 100 kN load cell

The testing of these lattice cubes was planned in a certain manner.

1. The first set of test were done by trying to load one sample along each direction till failure or high elongation (whichever comes first).
2. Using the failure mode to identify the point of yielding, a further hysteresis plot was built by doing cyclic loading of the parts in order to develop accurate E modulus values.
3. After finishing each loading cycle, another cycle with the same specifications was run on the same part, in order to remove the inaccuracies caused due to rough/non-parallel surfaces on the lattice cubes.

4.3 Experiment 3: Hydrostatic performance of cylindrical section

The third experiment was planned to predict the hydrostatic failure and establish the performance of the lattice structures being used as stiffeners, as compared to an empty shell with similar weight. The actual float is made up of several thin cylindrical sections which are then welded together with rings in between them. This experiment would attempt to prove the applicability of higher loads on AM stiffened structures, which would provide a much better property in hydrostatic loading when compared to normal part. The figure 4.5 reflect how the part would look like and some cut sectional views of the stiffened structures.

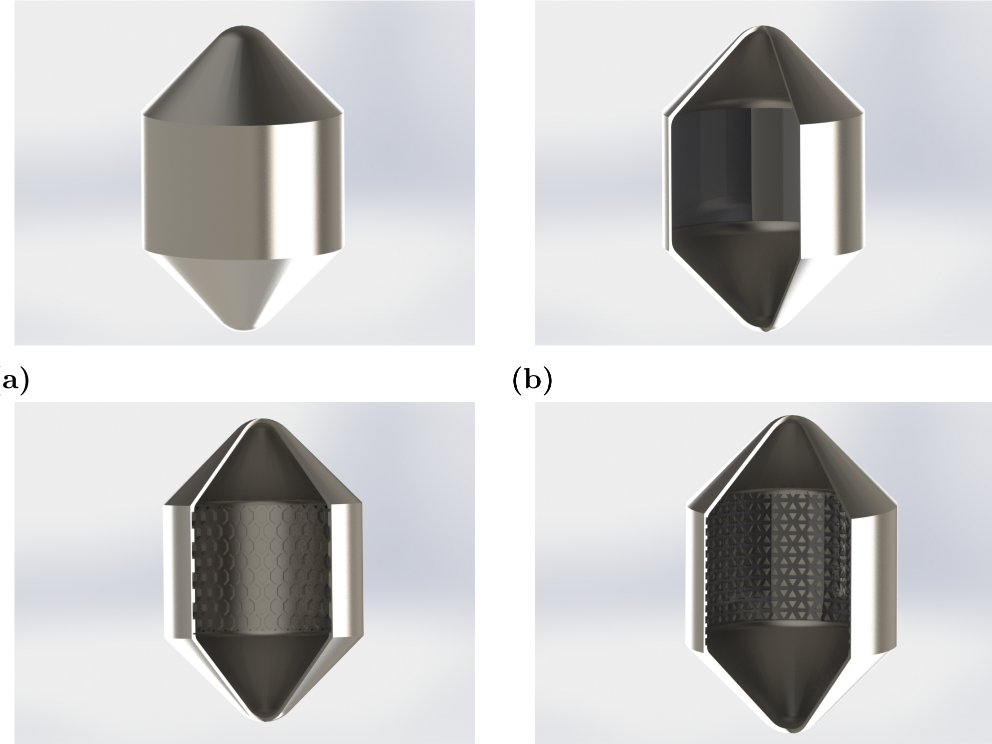

(a) (b)

(c) (d)

Figure 4.5: Cut section views of cylindrical sections designed to compare different stiffeners under hydrostatic loads: a) front view of the whole part; b) cut section view of actual section with thin walls only; c) cut section view of section with honeycomb stiffeners; d) cut section view of section with isogrid stiffeners

4.4 Experiment 4: Laser processing parameters evaluation

For thin shells, printing parameters might be different than those of parts with thicker sections. Attempts were made to print samples for experiment 1 and 2 at ABB and resulted in multiple failures. It was seen that the laser parameters affect the printability as much as the design, making the part susceptible to cracking, overheating, distortion and even crashing of prints. Hence, the printability aspect is added to the study, to quantify an optimised laser parameters for a certain thin shell. Some of the failed specimens after printing are shown in figure 4.6.

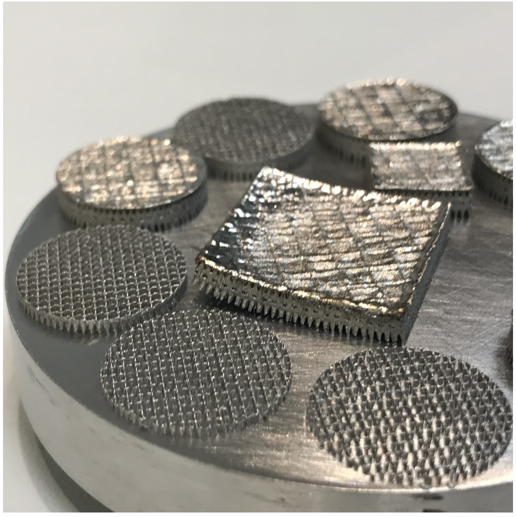

(a)

(b)

Figure 4.6: Different types of failures as seen during metal printing at ABB on a realizer SLM 50 printer: a) failed sample showing residual stress formation on build plate; b) failed sample which formed very rough surfaces on conical head

For this experiment, cylinders with a 10 mm outer diameter and 5 mm height were printed and the variables kept during the prints can be seen in table 4.1.

Table 4.1: Parameter changes planned during experiment 4; printer used was realizer SLM 50

Variable name	**Range**
Part thickness	0,4 mm , 1 mm
Laser power	60-120 W
Laser speed	250-750 mm/s
Layer thickness	20 μm , 40 μm
Hatching	Chessboard/chequered , shell

A total of 48 samples were planned based on design of experiments[21] using MODDE V11 software and implementing full factorial design (2^{nd} level) to develop all the qualitative and quantitative parameters. A first experiment of screening was done which was directly linked to the second experiment of evaluation. The screening experiment was to check if the part passed or failed during printing. It was seen that 10 parts out of 48 parts failed. A total of four prints were done on the machine, having all samples in two different thicknesses and different layer heights. At the end, it was planned to check these parts under a light optical microscope and plan a micro-structural and hardness evaluation as a post-thesis study.

5
Results and discussion

All the parts for experiments 1, 2, 3 were printed on a EOS M290 printer and 20 μm layer thickness at AMEXCI whereas the parts for experiment 4 were printed on a realizer SLM 50 printer at ABB with different layer thicknesses.

5.1 Experiment 1

During uniaxial compression of the thin cylindrical shells, it was observed that the critical load parameter improves when the thickness of the cylindrical section was increased. This makes sense intuitively since a thicker column should take higher loads. The buckling failure was simulated in ANSYS followed by actual experimental results. Results were further compared, as will be discussed below.
The boundary conditions for these simulations were modified in order to replicate the exact case scenario of the failure observed during testing. For example, 8124 N was kept as simulated load value since that was seen to be the average load at which first mode of buckling was observed in the parts of 0,4 mm thickness. Similar values were taken from average failure loads of other thicknesses to simulate them. The mesh used was a 0,2 mm shell mesh for the cylindrical section along with a 1 mm solid mesh for the solid part at top and bottom. This was done to make the simulations consistent to the real life result. The simulation results for a 0,4 mm thick cylindrical section can be seen in figure 5.1.

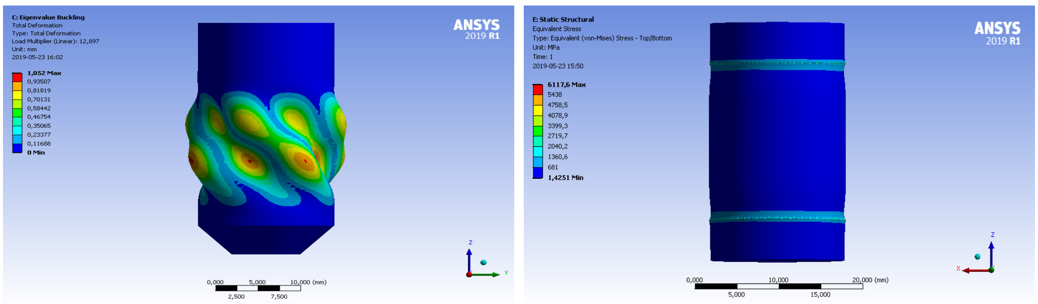

(a) **(b)**

Figure 5.1: ANSYS results showing Euler buckling test results and static structural testing results: a) Euler buckling showing the theoretical factor of safety to be 12,9 at 8124 N uniaxial load and 0,4 mm thickness at cylindrical section; b) stress generated at 8124 N in the part, showing the average stress value in the range of 401 MPa at the 0,4 mm thickness

A curve reflecting the load-deflection curve for all the 15 parts tested (five parts for each thickness) is shown in figure 5.2.

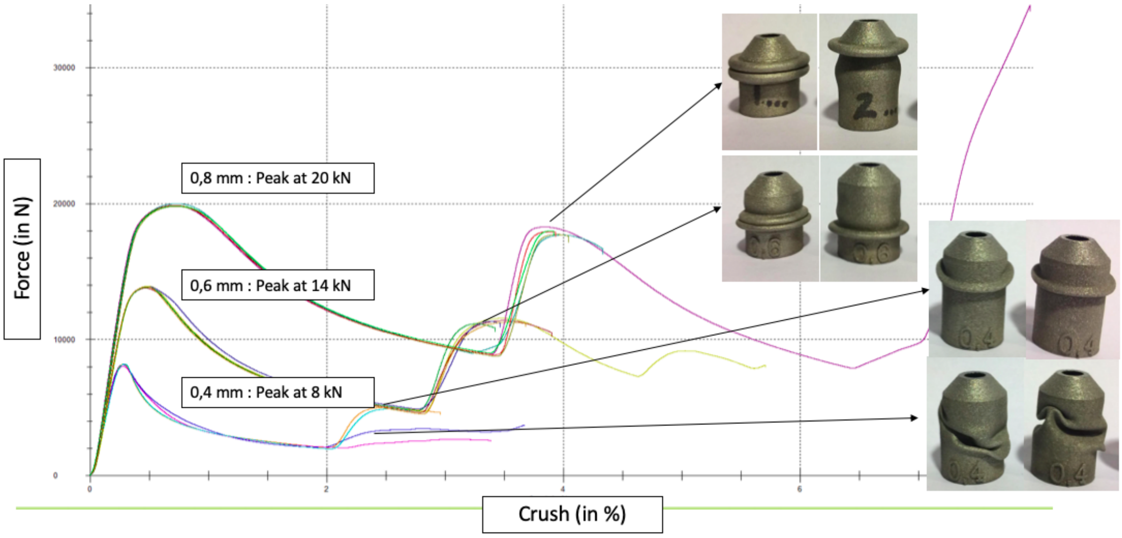

Figure 5.2: Uniaxial compression test results for cylindrical sections of different section thicknesses showing the average peak load

The figures 5.3, 5.4 and 5.5 reflect the buckling in case of the parts of different thicknesses with respect to actual part (on the left most side in each image).

Figure 5.3: Buckling results on cylindrical sections with thickness of 0,4mm

Figure 5.4: Buckling results on cylindrical sections with thickness of 0,6mm

Figure 5.5: Buckling results on cylindrical sections with thickness of 0,8mm

From experiment 1, the graph for the experimental vs theoretical non-linearity in the parts is shown in figure 5.6. This graph is a representation of how the linear buckling results from ANSYS were taken and extrapolated to form a theoretical non-linear performance based on [6]. The same was then compared with the experimental results.

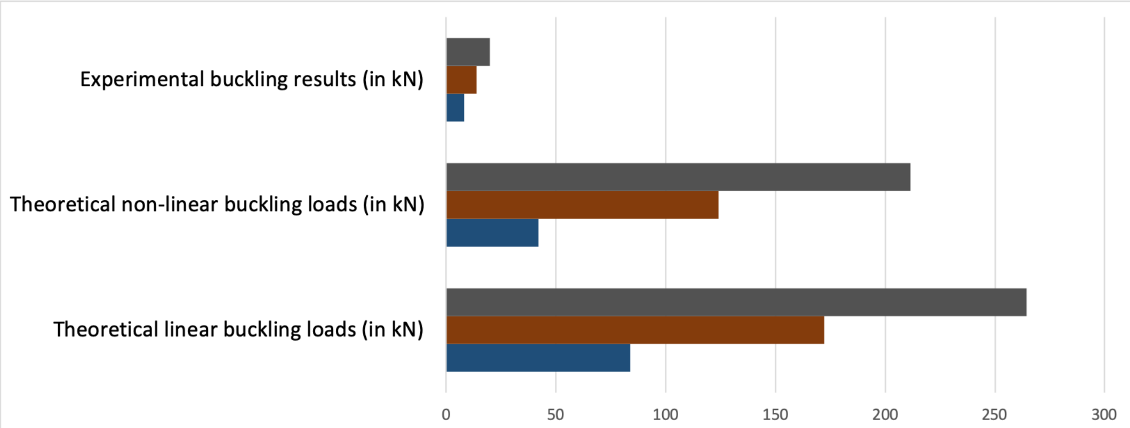

	Theoretical linear buckling loads (in kN)	Theoretical non-linear buckling loads (in kN)	Experimental buckling results (in kN)
0,8 mm	264,22	211,376	19,889
0,6 mm	172,17	123,9624	13,883
0,4 mm	83,742	41,871	8,124

Figure 5.6: A graph representing the non-linearity from Euler buckling, both theoretically and experimentally where expected non-linearity shows the theoretical results and actual non-linearity shows the experimental results

This shows that although theoretical predictions suggest a non-linear behaviour, the actual results reflect a much lower linear value at which buckling occurred. This could either be related to material failure occurring before the theoretical Euler buckling loads or surface roughness affecting the Euler buckling loads in a worse manner than expected.

5.1.1 Material failure before Euler buckling

The stresses calculated at buckling loads corresponded to the yield strength values of 316L stainless steel[7]. This was an interesting observation since [22] indicates that Euler buckling is only applicable in the elastic region, and this test proves that. Thus, as soon as the yield stress is reached, the material fails plastically and is unable to take the critical loads as calculated in Euler's formula. These stresses could be simulated quite accurately, as shown in Figure 5.7.

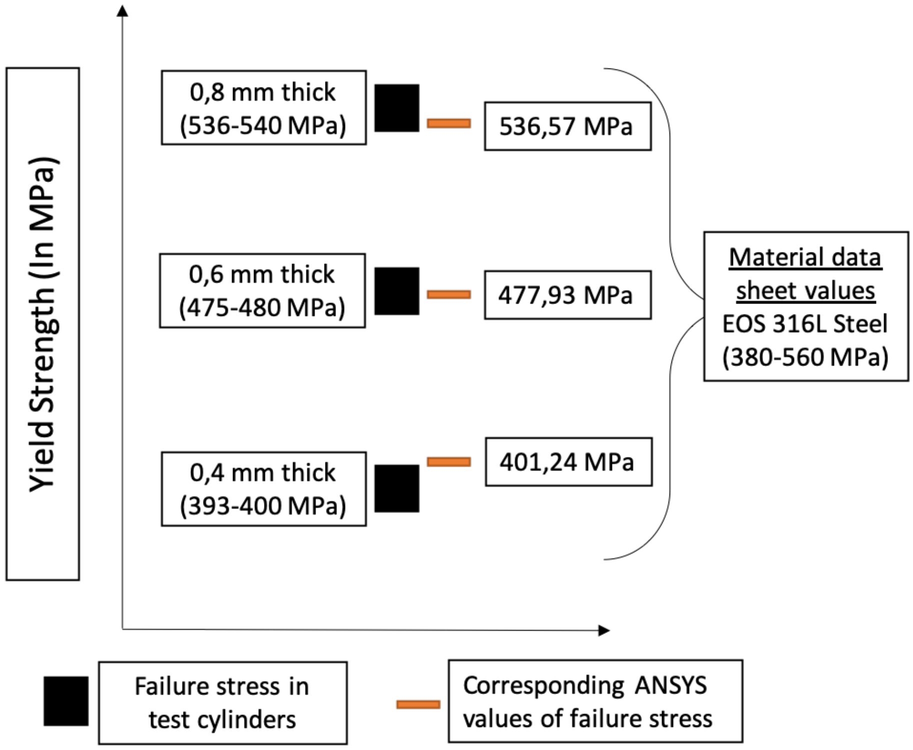

Figure 5.7: Graph representing the simulated values of stresses generated in ANSYS models vs experimental values of stresses when critical buckling loads were applied

5.1.2 Non-linearity co-relation with surface roughnesses

As per [7], a surface roughness (R_z) of 80±20 μm on as-printed and 30±10 μm after shot peening can be expected along Z direction, if the part is printed using 20 μm layer height. It was expected that the same would cause a detrimental effect on the buckling of the part, since the surface roughness to thickness of the part increases if the thicknesses are decreased from 0,8 mm to 0,4 mm. Surface roughness is also expected to induce inaccuracies in the buckling load values, creating a scatter. However, not much of scattering was observed and the experimental range was consistent between 7,53-9,7% of linear loads, which is better than the theoretical range of 50-80% of linear load. Hence, it seems like the effect of surface roughness is minimal on the part. The same is depicted in figure 5.8. It is important to note that the surface roughness was not measured in this work and parts were printed using parameters for the high surface finish, with the layer thickness of 20 μm, meaning that much better surface finish than mentioned in [7] should be expected.

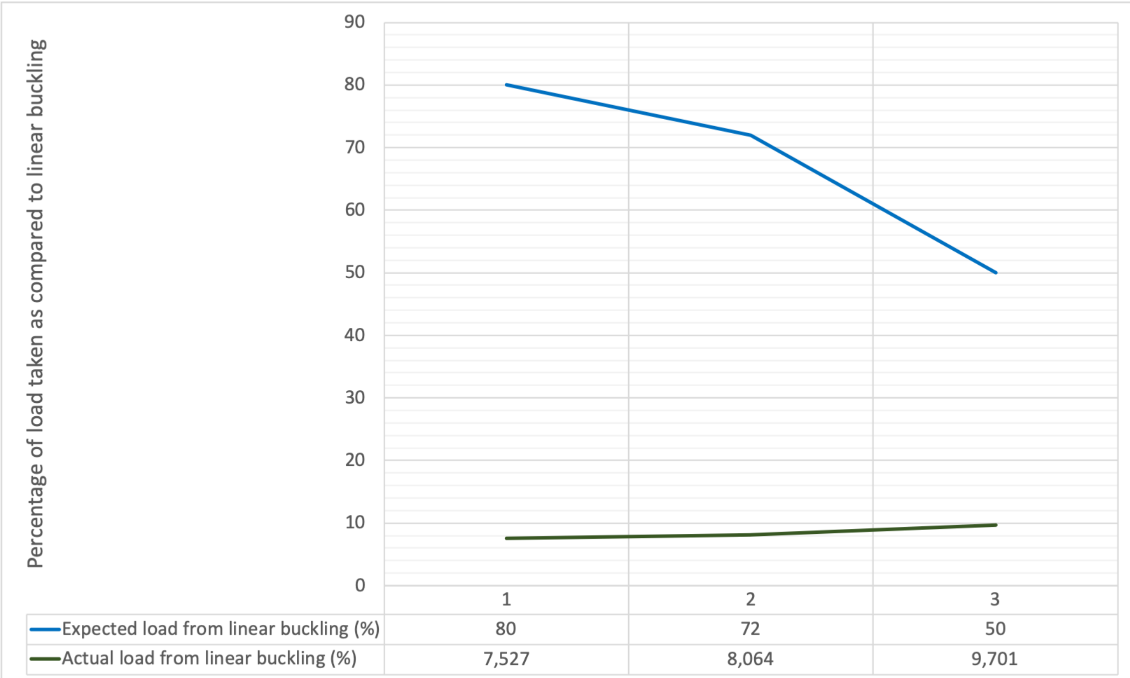

Figure 5.8: Graph representing the ratio of non-linear and linear buckling loads on y-axis for three different thicknesses of cylindrical cross sections (from 0,8 mm thick to 0,4 mm thick)

5.2 Experiment 2

The second experiment was conducted to study the directional properties of lattice structures. Since the lattice structures are being used as stiffeners, it is quite important to know how much of a strengthening effect they provide in X, Y and Z directions. Two lattice structures were simulated out of the ones studied. Honeycombs and isogrids were tested in ANSYS at similar design conditions, till elasticity limit (0,2% strain, or yield limit) using a displacement controlled load. The mesh was kept to be a solid mesh of 0,5 mm and the results are shown in figures 5.9 and 5.10. The parts were designed in a way, to have a thick solid block on top and bottom, similar to a compression plate. Figure 5.11 shows the relative density of the lattice cubes with respect to a solid block of steel.

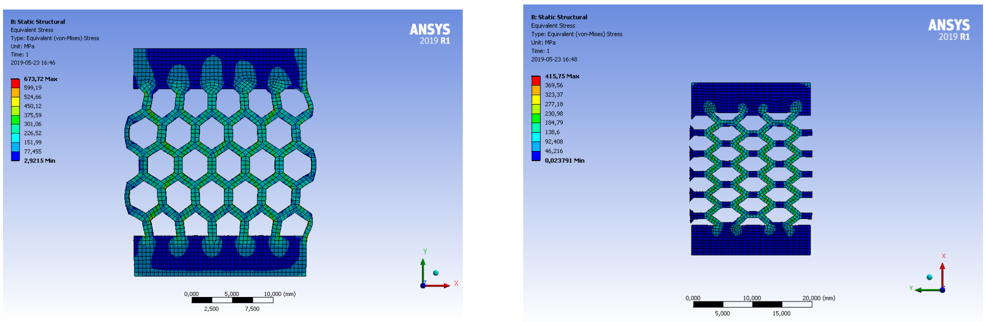

(a) (b)

Figure 5.9: ANSYS simulation for elastic deformation of honeycomb lattice cubes: a) stresses generated on honeycomb lattice cubes along Z direction; b) stresses generated on honeycomb lattice cubes along XY direction

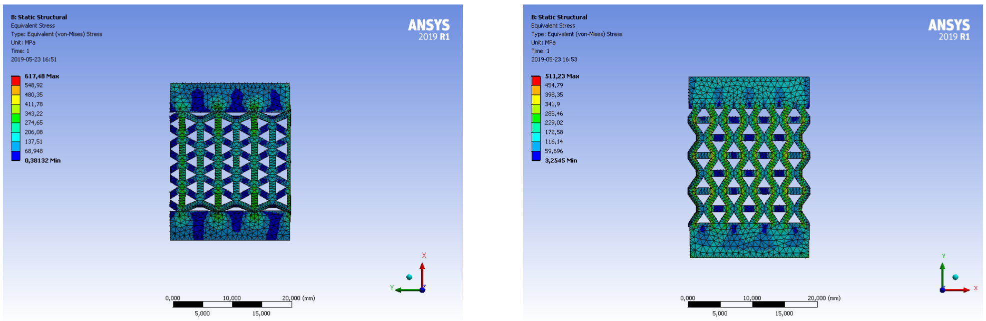

(a) (b)

Figure 5.10: ANSYS simulation for elastic deformation of isogrid lattice cubes: a) stresses generated on isogrid lattice cubes along Z direction; b) stresses generated on isogrid lattice cubes along XY direction

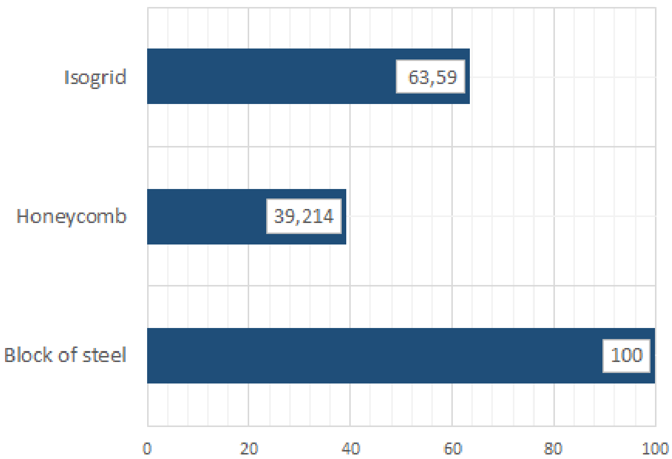

Figure 5.11: Relative density (in %) of lattice cubes with respect to solid block of 316L steel

The figure 5.12 shows experimental compression load-displacement curves of different lattice cubes in different directions of testing. Figures 5.13 and 5.14 show pictures of different lattice samples before and after loading under uniaxial compression in different directions.

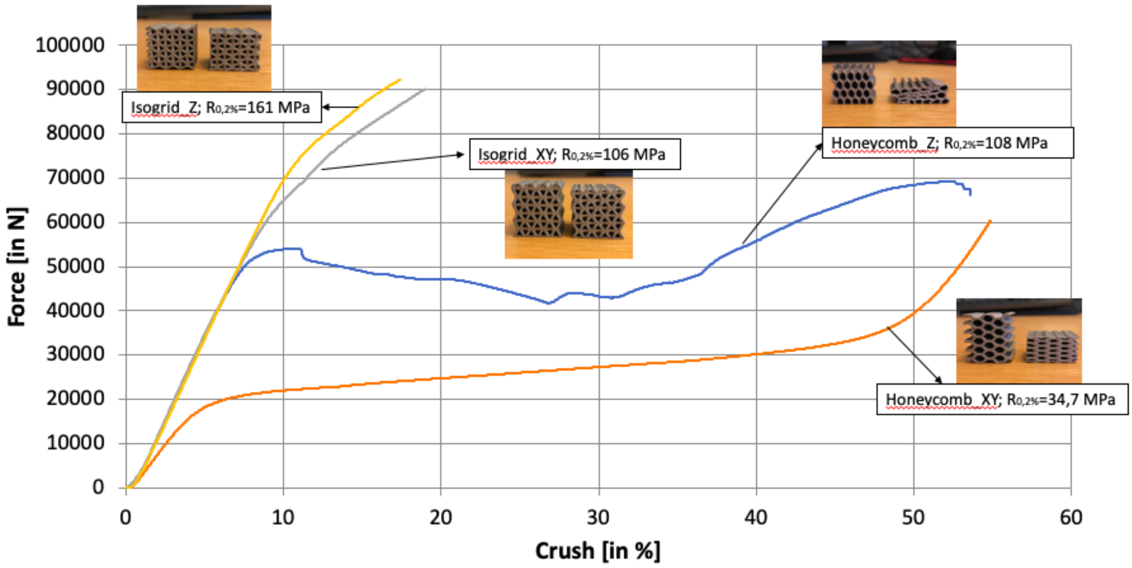

Figure 5.12: Uniaxial compression test results for different lattice cubes along different directions reflecting the average yield strength R0,2%

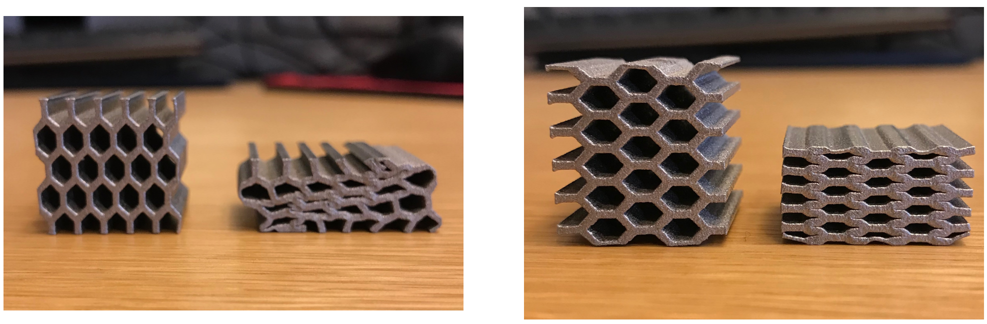

(a) (b)

Figure 5.13: Honeycomb lattice crush results (before and after crushing): a) before and after of the honeycomb lattice after being loaded along Z direction; b) before and after of the honeycomb lattice after being loaded along X direction

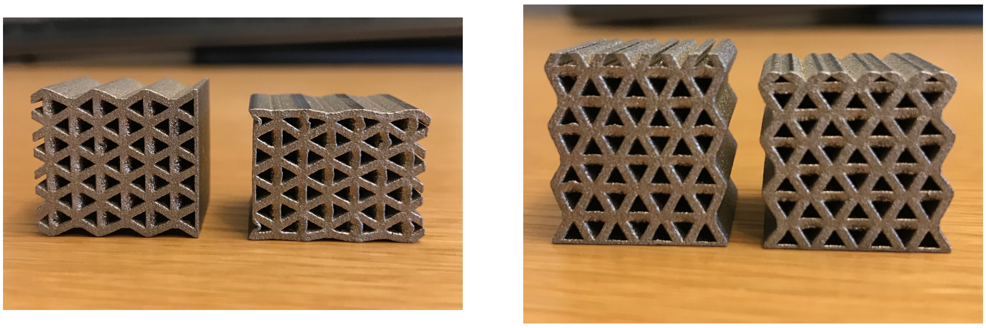

(a) (b)

Figure 5.14: Isogrid lattice crush results (before and after crushing): a) before and after of the isogrid lattice after being loaded along Z direction; b) before and after of the isogrid lattice after being loaded along X direction

After testing lattice cubes experimentally, the simulation results were compared for both yield strength and the young's modulus for these parts. The figures 5.15 and 5.16 reflect the value of the theoretical vs experimental values of the Young's modulus (in MPa) and yield strength (in MPa).

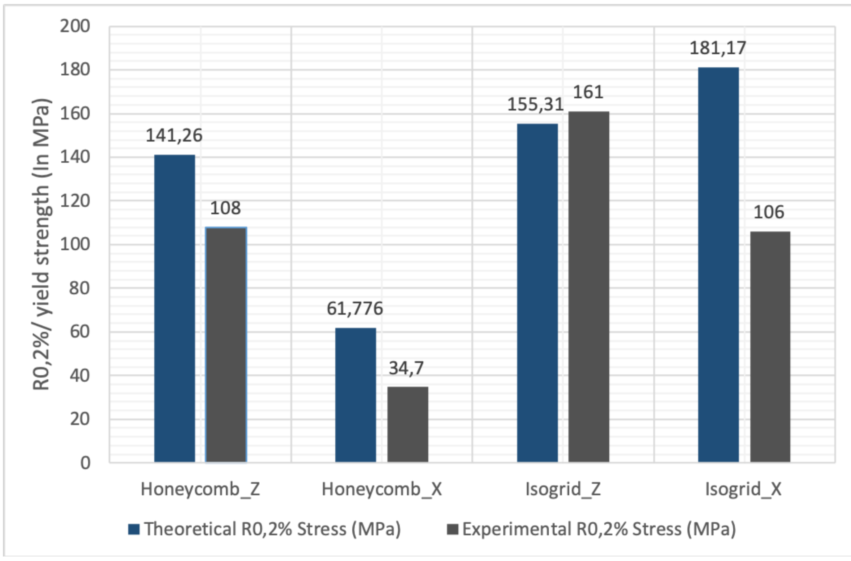

Figure 5.15: Graph representing the theoretical vs experimental values for yield strength (in MPa) for different lattice structures studied

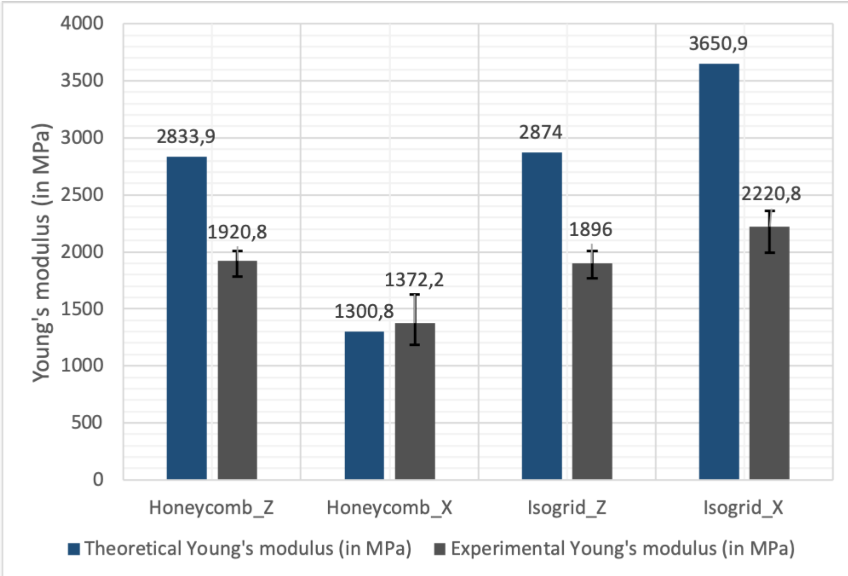

Figure 5.16: Graph representing the theoretical vs experimental values for young's modulus (in MPa) for different lattice structures studied

It is believed that these differences between theoretical and experimental values comes from the defects and surface roughnesses in the parts. Another possibility could be the inaccuracies in simulations, pointing out that the mesh should be better defined for these load conditions. More samples should be tested to estimate scatter of test values. In addition, dedicated study of the microstructure and, when possible, fracture surface of the tested samples should be performed to study the defects causing failure of the component. After compiling these data values, two different structures can be simulated, characterised by different properties in all three directions. The expected yield strength and Young's modulus values for these new honeycomb and isogrid structures are shown in figure 5.17.

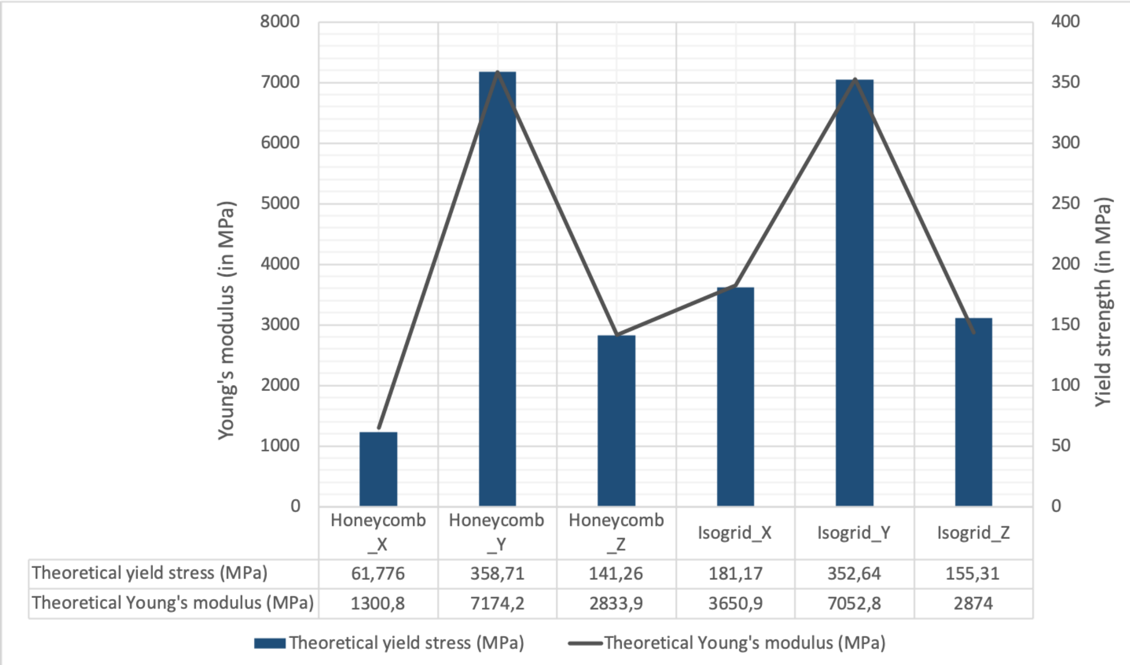

Figure 5.17: Graph representing the expected elastic properties for new lattice structures

It can be concluded that these structures do not lose the strength values in Y direction, even though they are left with only 40-65% of the material in them. This direction is considered to be the strengthening direction and helps the part to achieve it's stiffness during buckling. If the load-displacement curve for lattice materials are referred to again (figure 5.12), rather large differences between different directions can be seen. The observations can be summarised as follows:

1. The honeycombs could elongate beyond 50% elongation. This would not be possible in a real life scenario, since the part would fail/buckle before that.
2. The testing of isogrid structure shows properties above the physical possibilities of the experimental setup since the maximum load cell value of 100 kN was reached without structure failure and hence testing had to be stopped.

Based on these observations, it can be said that the lattice structures can be tweaked to provide better directional properties in Z and Y directions where it is mostly required and remove more material. However, part has to be tested in real or simulated conditions to prove the concept proposed.

To get consistent Young's modulus values, step-wise cyclic loading was conducted. For example, honeycomb lattices along Z direction were loaded incrementally (10 kN, 20 kN, 30 kN and 40 kN loads) until until the yield point and then unloaded, see figure 5.18. The process was repeated a second time and it was seen that the curve shifts leftwards, because the part seemingly gets flatter with respect to the compression plates. However, the Young's modulus (E) values, which is reflected by the slope of these curves, stays quite constant.

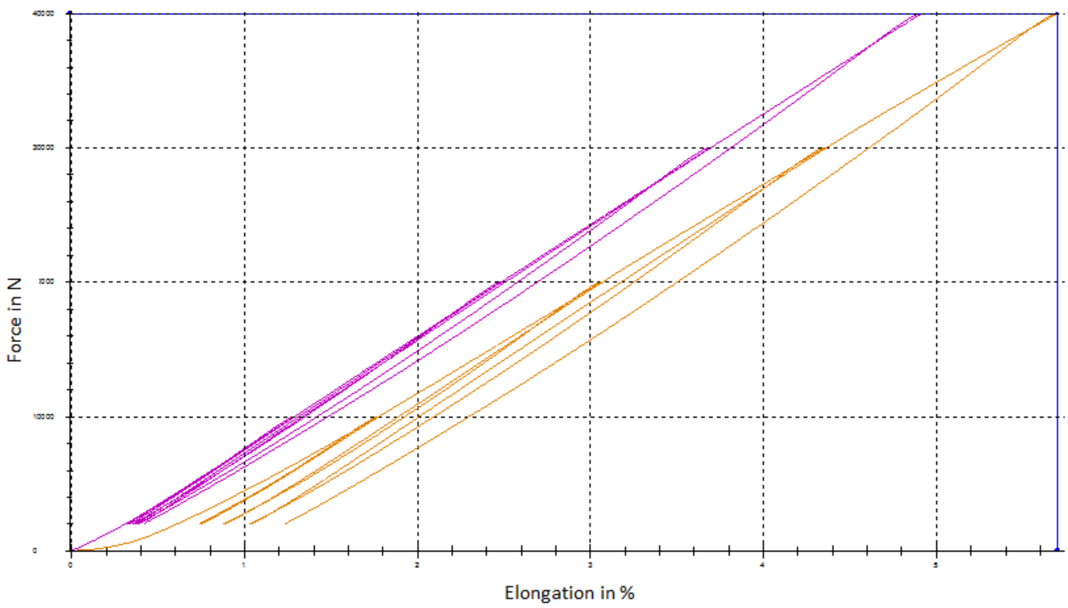

Figure 5.18: Variation in elongation during loading/ unloading of honeycomb lattice specimen during cyclic compression test to define elastic properties

5.3 Experiment 3

The test for hydrostatic performance of cylindrical sections showed improved simulation results for the stiffeners as well. However, it is important to note that the meshes generated for the honeycomb and isogrid parts were not hexahedral mesh of 1 mm, since the part had very fine and intersecting surfaces, making it hard to solve the mesh. So, a normal quadratic mesh (with tetragonal elements) was taken for these parts. This can have some sources of error in final solution. Actual tests have not yet been conducted since the equipment was unavailable and the parts took longer than expected to print. Hence, the simulation results were only discussed. Hydrostatic buckling of tubes with and without different stiffeners under 1 MPa hydrostatic load is shown in figures 5.19, 5.20 and 5.21.

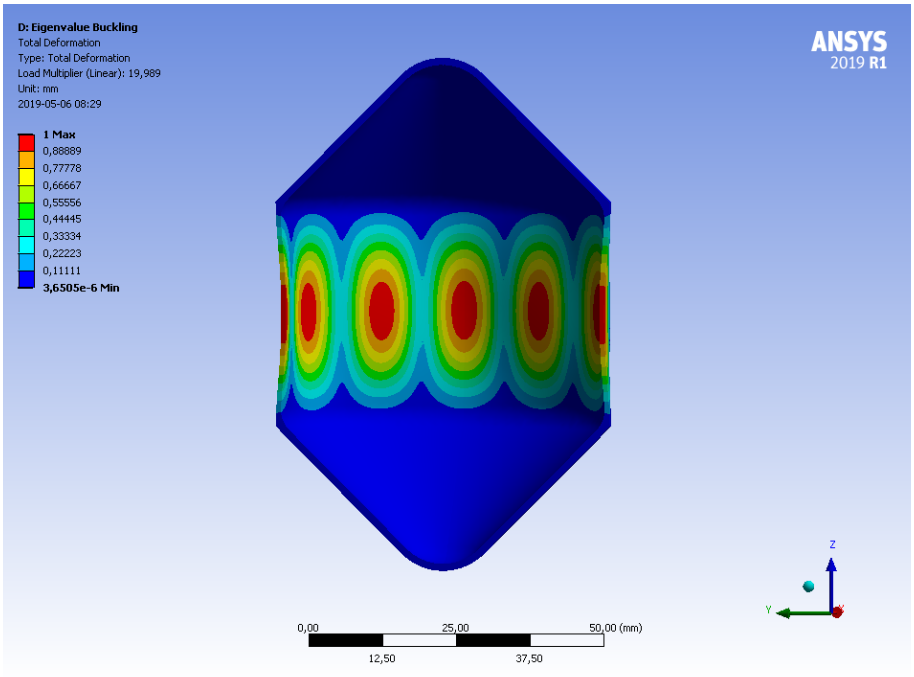

Figure 5.19: Hydrostatic buckling of an empty tube without stiffeners

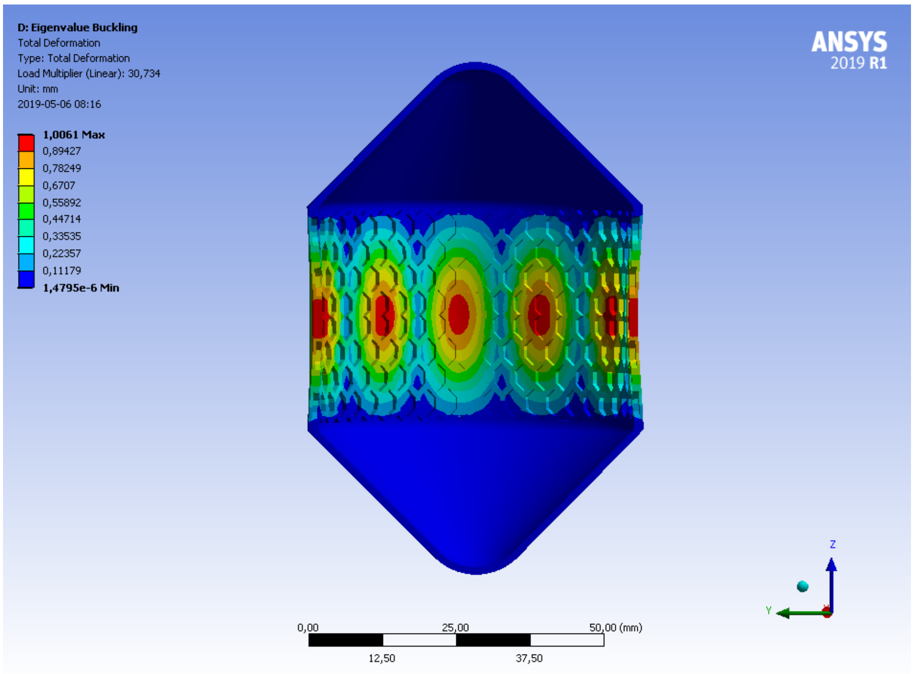

Figure 5.20: Hydrostatic buckling of an empty tube with honeycomb stiffeners

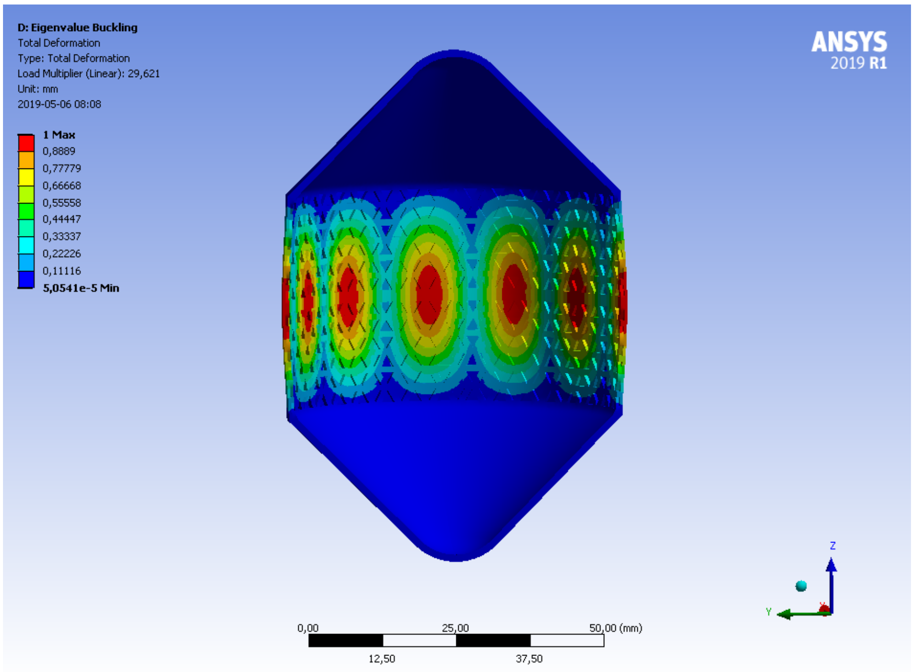

Figure 5.21: Hydrostatic buckling of an empty tube with isogrid stiffeners

The resultant hydrostatic performance of the different tubes is represented in figure 5.22.

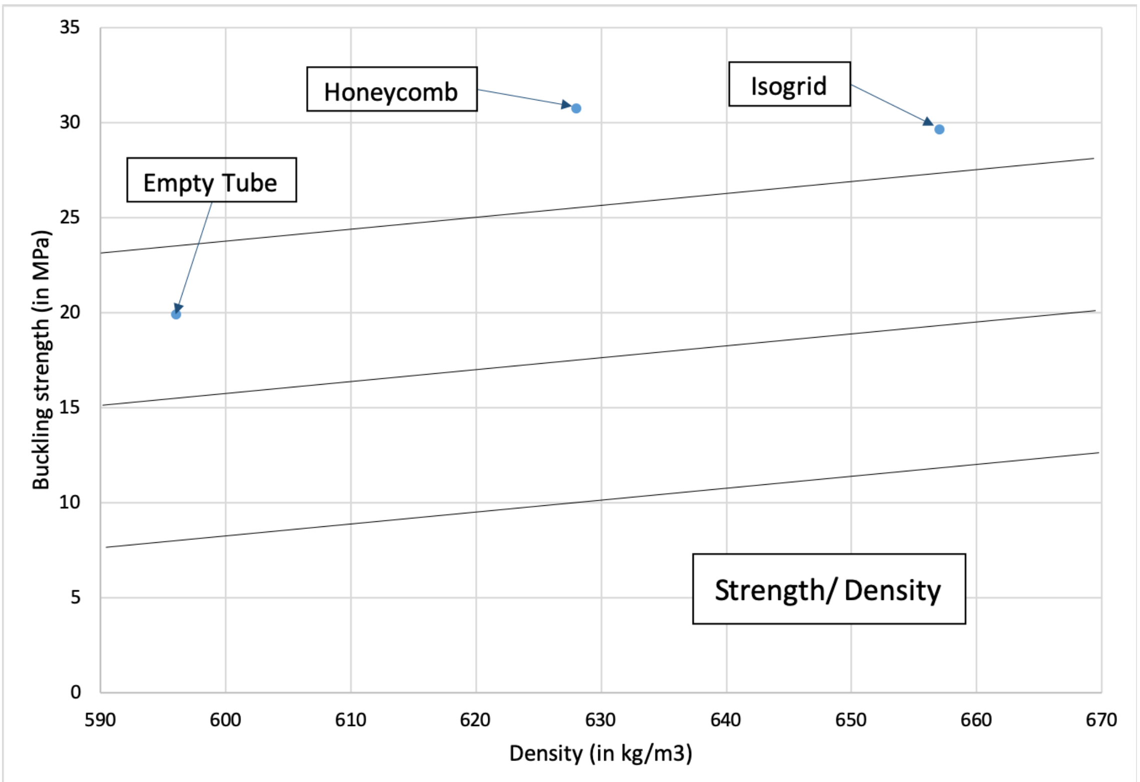

Figure 5.22: Comparison of strength/density performance of different stiffeners under hydrostatic loads, in an Ashby chart[8]

The simulation results for these experiments were only shown since the actual tests could not be conducted. This experiment was simulated to show how the stiffeners enhance critical buckling strengths. Simulation results show that around 50% improvement in specific strength can be expected in a stiffened sections as compared to unstiffened section. This would mean that when this would be combined with hollow rings, it would lead to a multiplication effect in improvement of performance. Figure 5.23 shows the cross-section of one of such sections, printed in stainless steel.

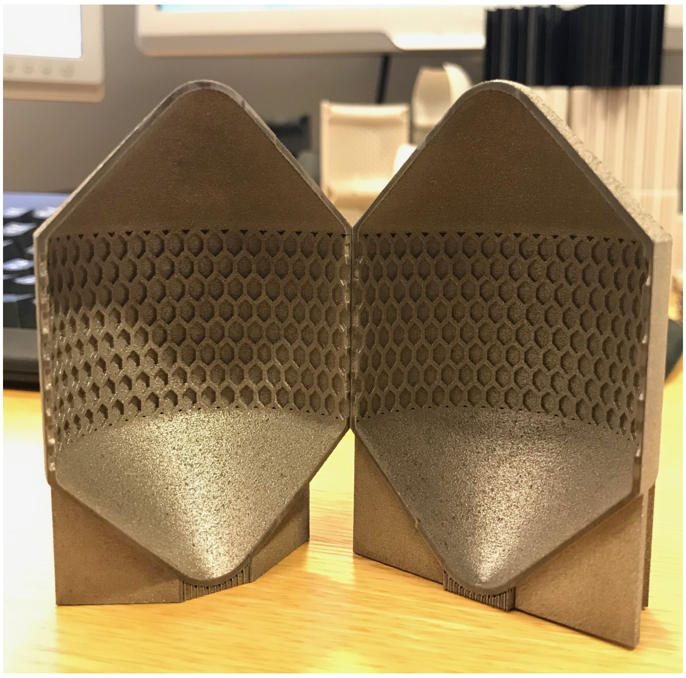

Figure 5.23: Cross-section of one of the parts showing the stiffener inside the part

5.4 Experiment 4

This experiment was planned in order to establish the reason for the build failure during LPBF processing, observed during printing samples for the experiments, described above. Since this experiment was conducted on a smaller SLM 50 printer instead of a EOS M290, results may vary. However, a trend could be developed using this experiment, which will be generic. The approach to design of experiments was utilised for making the samples and one of the design of experiment (DOE) graph is described in figure 5.24.

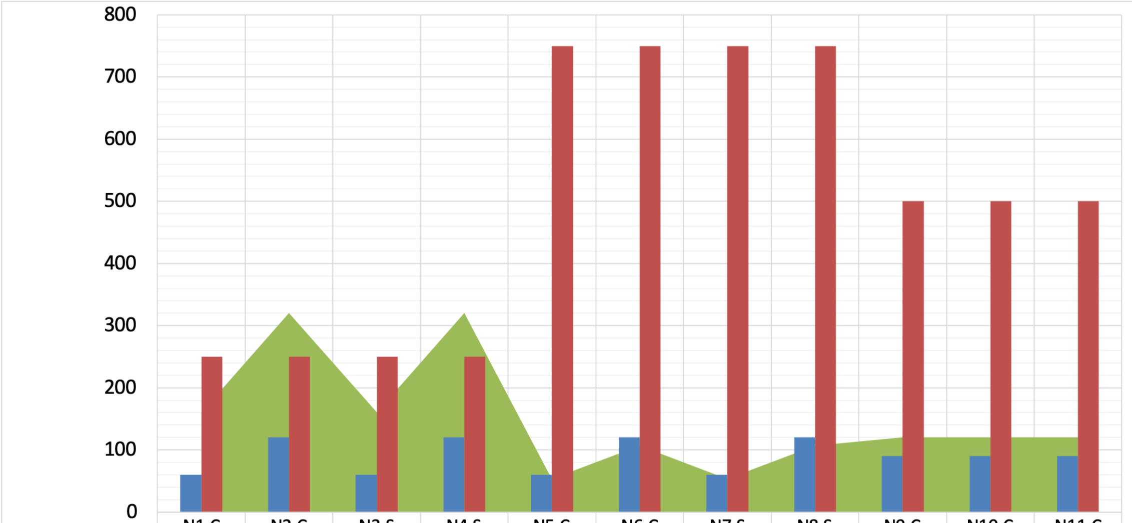

	N1 C	N2 C	N3 S	N4 S	N5 C	N6 C	N7 S	N8 S	N9 C	N10 C	N11 C
Energy Density (In W/mm3)	160,00	320,00	160,00	320,00	53,33	106,67	53,33	106,67	120,00	120,00	120,00
Laser Power (In W)	60	120	60	120	60	120	60	120	90	90	90
Laser Speed (In mm/s)	250	250	250	250	750	750	750	750	500	500	500

Figure 5.24: Test number 1 based on DOE of experiment 4

Figure 5.24 shows the different parameters such as laser power and laser speed chosen for different samples. Additionally, one of the build plates, after printing and removal of powder, is shown in figure 5.25.

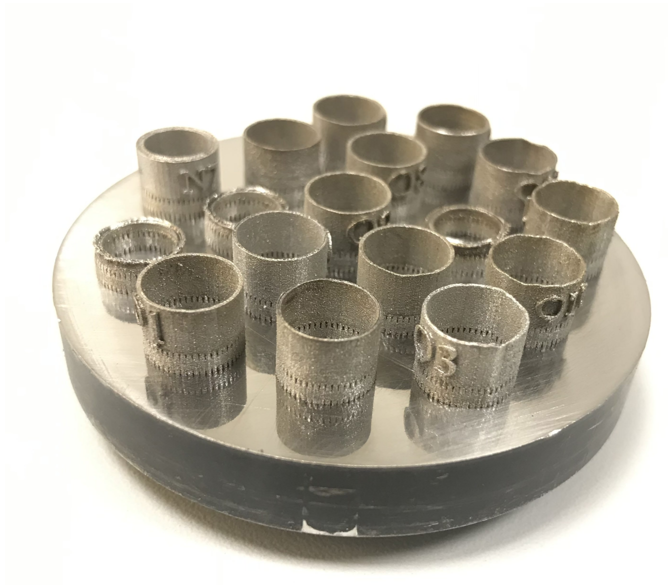

Figure 5.25: Build plate number 4 for experiment 4, right after printing and removal of excess powder; printed on realizer SLM 50 printer at ABB

After design of experiments and producing 38 successful samples, some of these were studied under a light optical microscope to see the effect of laser parameters on them in order to identify the changes between different printing parameters. Two examples that showed the largest differences are discussed below:

1. Difference between chequered scan strategy and shell scan strategy:
   The scan strategies used for thin shells were chequered patterns in X, Y directions in alternate layers and forming small islands of scan patterns, which are 4,05 mm x 4,05 mm in size for each island. These islands are a general scan strategy used and was mostly successful for different thicknesses, layer heights and energy densities. The shell scan strategy, where the laser path follows the circumference of the shell, was seen as an intuitive strategy to induce less distortions and decrease in localised heat. Components produced by different scan strategies can be seen in figure 5.26, as observed by light optical microscope at low magnification.

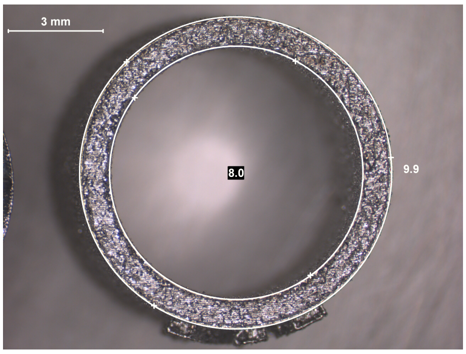

(a)

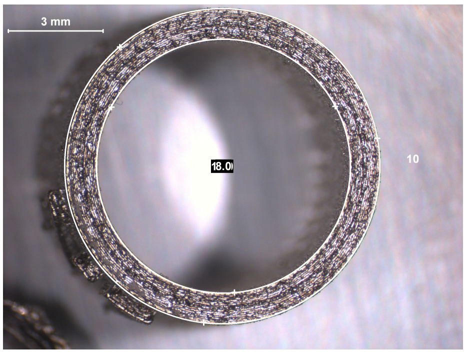

(b)

Figure 5.26: Top layer view of components produced using varying scan strategies for printing thin shells when observed under a light optical microscope at low magnifications: a) chequered scan strategy and b) shell scan strategy

2. Difference between low and high energy densities:
   There was another peculiar difference observed in parts having very low or high energy densities. The low energy densities formed rough top surface texture whereas the one with high energy density formed small holes in the surface, probably large key-hole porosity. The sample with high energy density also exhibited complete melting on the surface. Appearance of samples at low magnification can be seen in figure 5.27.

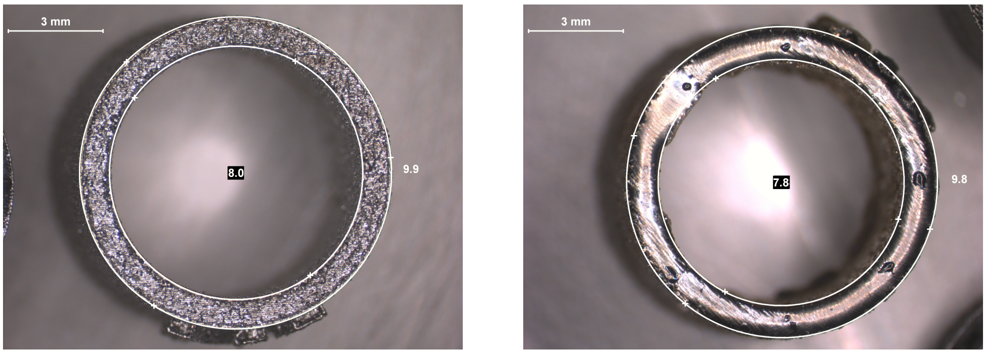

(a) **(b)**

Figure 5.27: Top layer view of the components produced using different energy density when observed under a light optical microscope at low magnification: a) low energy density (53,33 W/mm^3) and b) high energy density (320 W/mm^3)

The work presented in this section was done as a post-thesis work in order to understand better of the effect of the laser processing parameters. It was observed that if the process parameters are well-controlled while printing a thin shell (having diameter:thickness ratios of $>$ 20:1), a higher consistency in printing of thin shell structures could be expected. A more detailed study would thus benefit the mass manufacturing of this product, along with providing ABB with some research insight into thin shell structures. This is recommended to be performed using production machines as example EOS M290, where final components were printed, as results are not directly transferable between between different hardwares.

6
Conclusions

The major benefits of AM for the component studied can be summarised as follows:

1. Printability of the part
   (a) The part design was based on careful consideration of DfAM principles such as print orientation and ensuring best retention of circularity of the tube.
   (b) The thin walls and the lattices/stiffeners would support each other during the prints, making the part more stable and the design more robust.
   (c) Printing vertically requires minimal supports, thus the parts can be printed as "net shape" and have less material wastage.
   (d) The weldability of the part was considered while printing, since the fillets at the hollow rings have thicker sections (about 1,5 mm) than the original part, thus making it easier to weld.
   (e) Spherical section may be hard to print accurately without supports. A good idea could be to print a thicker sphere and machine it afterwards to desired thickness. On the other hand, more work on support structures can be done, to improve printability.
2. Simulation of performance: The simulation results showed about 3 times improvement in specific buckling strength in one of the designs - isogrid stiffened AM part with hollow rings, as can be seen in table 6.1. The stress levels shown were well below the ultimate strength of the material, which means that the idea might work. However, this design concept has to be proven experimentally.

Table 6.1: Table showing improvement in specific strength for different floating device designs

Design name	**Increase in strength/ density ratio**
Original part	1
Thicker rings	1,53 times original part
AM isogrid	3,14 times original part
AM honeycomb	2,31 times original part

3. Modular designs possible:
   (a) These floating devices take modularity to the next level, by giving an opportunity for optimisation of lattice based stiffeners and hollow rings to define "new materials". Hence, strength to weight ratios can be adjusted to become as high as aluminium or as low as some plastics.

   (b) AM gives the opportunity to print several parts together on the same build plate, thus giving another freedom in manufacturing.
4. Consolidation of parts:
   (a) For this case study, the original part had 13 parts welded together whereas the proposed design allows to make a better product with 3 parts welded together.
   (b) There are future possibilities of having some kind of consolidation for the extra weight that is required as per design, by having design accounting for these extra weights, or bimetallic prints possible.
5. Topology optimisation:
   (a) The hollow ring concept has not been elaborated. They can be developed by using a strong topology optimisation software that changes the shape of the part based on the maximum allowable stresses.
   (b) The stiffeners such as isogrids and honeycombs can be improved by changing the shape to other grid-based structures.
6. Material definition:
   (a) The material definition has been taken along Z direction after stress relieving, which means that the most conservative values were assumed while designing the part. This assumption might affect the actual performance of the part, since in reality the material is anisotropic.

Having said all these benefits, AM is prone to some shortcomings as well, which cannot be overlooked without actual printing and experimental evaluation:

1. Non linearity in buckling:
   (a) The effect of non-linearity is very important since it can completely change the performance of the part. Thus, it needs more experimental proof before being sure of the design.
   (b) The thin shell design with stiffeners has not been proven before. Such thin shells with large diameters of about 60 mm and skin thicknesses of sub millimetre are very complicated to manufacture and thus induces more non-linear buckling effects.
2. Number of edges increase due to lattice stiffeners:
   (a) It might seem that the lattice stiffeners are a good idea. However, they might increase edges in the part exponentially which act as sites for stress concentration. This can lead to poorer performance of the part.
   (b) The lattice structures need to be printed separately and tested several times to develop a robust design.
3. Mesh analysis on product :
   The current mesh analysis done on the part is not up to professional standards. There can be cleverer ways to simulate the same with less computation power and still use a finer mesh, to get results closer to reality. Also, AM parts are highly susceptible to differ in performance to what is mentioned on data sheets due to inconsistencies in prints as discussed before.

7

Future Work

Some suggestions on future work are also provided below:

1. Optimisation of stiffeners and rings The stiffeners and rings were optimised for a few iterations (probably 35-40 iterations). The load path during hydrostatic buckling can be understood and much better stiffeners can be developed using softwares for topology optimisation. There is also follow up literature available for design of structures such as isogrids, anisogrids etc., which might be helpful to suggest even better structures.
2. Laser process simulations accounting for non-linearity
   (a) It can be really helpful during development phase to understand what kind of laser processing parameters affect the printing of these parts and try to perfect them.
   (b) The non-linearity effect worsens due to inconsistent prints, considering that this part deals with such thin walls.
3. Readiness for mass manufacturing
   (a) To make these high-performance parts perform well under the current scenario, it is highly recommended to conform to standards such as ASME codes for materials. Thus, an intensive study to understand the applicability of such products in the ASME (or equivalent international codes) is essential to develop a product more suitable for a business case.
   (b) An analysis into the chemical reaction of different fluids with metals such as aluminium or 316L stainless steel[23] is crucial in order to be sure of how good will the product printed in 316L stainless steel perform.

List of Figures

List of Tables

Bibliography

[1] H. Bensoussan. The history of 3d printing: 3d printing technologies from the 80s to today. [Online]. Available: https://www.sculpteo.com/blog/2016/12/14/the-history-of-3d-printing-3d-printing-technologies-from-the-80s-to-today

[2] Iso/astm 52900 (2015) standard terminology for additive manufacturing - general principles - terminology.

[3] K. Laszlo, P. Springer, och G. S., *Mechanics of Composite Structures.* Cambridge University Press, 2003.

[4] W. Gautschi. (2007) Leonhard euler:his life, the man, and his works. [Online]. Available: https://www.cs.purdue.edu/homes/wxg/EulerLect.pdf

[5] Elastic buckling. [Online]. Available: http://homepages.engineering.auckland.ac.nz/~pkel015/SolidMechanicsBooks/Part_I/BookSM_Part_I/07_ElasticityApplications/07_Elasticity_Applications_05_Buckling.pdf

[6] J. Amdahl. Buckling and collapse of marine structures in steel and aluminium. [Online]. Available: https://www.ntnu.edu/studies/courses/TMR4205/2018/1#tab=omEmnet

[7] Material data sheet for eos stainless steel 316l. [Online]. Available: https://cdn1.scrvt.com/eos/77d285f20ed6ae89/dd6850c010d3/EOSStainlessSteel316L.pdf

[8] (2019) Ces edupack software, granta design limited, cambridge, uk. [Online]. Available: https://www.grantadesign.com

[9] Dmls schematic setup. [Online]. Available: https://commons.wikimedia.org/wiki/File:Selective_laser_melting_system_schematic.jpg

[10] Ebm schematic setup. [Online]. Available: http://www.arcam.com/technology/electron-beam-melting/hardware/

[11] V.-P. Matilainen, J. Pekkarinen, och A. Salminen, “Weldability of additive manufactured stainless steel,” 2016.

[12] N. Li, S. Huang, G. Zhang, R. Qin, W. Liu, H. Xiong, G. Shi, och J. Blackburn, “Progress in additive manufacturing on new materials: A review,” 2018.

[13] Additive manufacturing : A game changer for the manufacturing industry? [Online]. Available: https://www.rolandberger.com/publications/publication_pdf/roland_berger_additive_manufacturing_1.pdf

[14] Design for metal am - a beginner’s guide. [Online]. Available: https://resources.renishaw.com/en/details/educational-article-design-for-metal-am-a-beginners-guide--101490

[15] D. Waltona och H. Moztarzadeh, “Design and development of an additive manufactured component by topology optimisation,” 2017.

[16] [Online]. Available: https://www.fastradius.com/resources/understanding-3d-printed-lattices-performance-and-design-considerations

[17] Crystal structures. [Online]. Available: https://web.iit.edu/sites/web/files/departments/academic-affairs/academic-resource-center/pdfs/Crystal_Structures.pdf

[18] M. Farahani, N. Hamta, A. Seifi, och M. A. Shirazi, "Reliability-based design optimization of composite shell structures," 2014.

[19] Dragon v2 interiors by spacex. [Online]. Available: https://en.wikipedia.org/wiki/SpaceX_Dragon#/media/File:Dragon_V2_interior.2.jpg

[20] Boeing cst 100. [Online]. Available: https://en.wikipedia.org/wiki/Isogrid#/media/File:CST-100_pressure_vessel.jpg

[21] L. Eriksson, E. Johansson, N. Kettaneh-Wold, C. Wikstrom, och S. Wold, *Design of Experiments*, 2008.

[22] X.-L. Zhao och G. Hancock, "Members subjected to bending and compression." [Online]. Available: https://www.sciencedirect.com/topics/materials-science/euler-buckling/pdf

[23] Graco, *Graco chemical compatibility guide*, 2013.

[24] Details on km26 magnetic level gauge : Abb. [Online]. Available: https://new.abb.com/products/measurement-products/level/magnetic-level-gauges/km26-magnetic-level-gauge

[25] B. M. Sauter, "Thesis report."

[26] Specific gravity. [Online]. Available: https://www.britannica.com/science/specific-gravity

[27] I. Gibson, D. Rosen, och B. Stucker, *Additive Manufacturing Technologies*. Springer, 2015.

[28] N. development institute. Welding of stainless steels and other joining methods. [Online]. Available: https://www.nickelinstitute.org/media/1854/weldingofstainlesssteelandotherjoiningmethods_9002_.pdf